Reactions of di- and polynuclear complexes. 9. Thermal, photochemical, and electrochemical activation of carbonyl ligands in an "M2C2S" cluster: CO substitution in [Fe2(CO)6{.mu.-(CF3)C2(CF3)S}] by tertiary phosphite, phosphines, and diphosphines. X-ray crystal structures of [Fe2(CO)6-nLn{.mu.-(CF3)C2(CF3)S}] (n = 1-3; L = phosphite)

Francoise Robin, Rene Rumin, Jean Talarmin, Francois Y. Petillon, and Kenneth W. Muir

Organometallics, **1993**, 12 (2), 365-380• DOI: 10.1021/om00026a023 • Publication Date (Web): 01 May 2002

Reactions of Di- and Polynuclear Complexes. 9.[1] Thermal, Photochemical, and Electrochemical Activation of Carbonyl Ligands in an "M_2C_2S" Cluster: CO Substitution in $[Fe_2(CO)_6\{\mu\text{-}(CF_3)C_2(CF_3)S\}]$ by Tertiary Phosphite, Phosphines, and Diphosphines. X-ray Crystal Structures of $[Fe_2(CO)_{6-n}L_n\{\mu\text{-}(CF_3)C_2(CF_3)S\}]$ (n = 1–3; L = Phosphite)

Françoise Robin, René Rumin, Jean Talarmin, and François Y. Petillon*

URA CNRS No. 322, "Chimie, Electrochimie Moléculaires et Chimie Analytique", Faculté des Sciences, Université de Bretagne Occidentale, BP 452, 29275 Brest-Cedex, France

Kenneth W. Muir*

Department of Chemistry, University of Glasgow, Glasgow G12 8QQ, Great Britain

Received May 21, 1992

The reactions of the cluster $[Fe_2(CO)_6\{\mu\text{-}(CF_3)C_2(CF_3)S\}]$ (1) with uni- and bidentate phosphines have been investigated. Carbonyl ligands are quantitatively displaced by 1 or 10 mol equiv of monophosphite or monophosphine in refluxed tetrahydrofuran, the only complexes formed under these conditions being the mono- and disubstituted products $[Fe_2(CO)_{6-n}L_n\{\mu\text{-}(CF_3)C_2(CF_3)S\}]$ (n = 1 (**2a** and **2b**); n = 2 (**3a** and **3b**); **a**, L = $(POMe)_3$; **b**, L = PPh_3). Formation of four different products $[Fe_2(CO)_5(L\text{-}L)\{\mu\text{-}(CF_3)C_2(CF_3)S\}]$ (**7**, L-L = dppm; **12**, L-L = dppe), $[Fe_2(CO)_4(\mu\text{-}L\text{-}L)\{\mu\text{-}(CF_3)C_2(CF_3)S\}]$ (**8** (dppm), **13** (dppe)), $[Fe_2(CO)_4(L\text{-}L)\{\mu\text{-}(CF_3)C_2(CF_3)S\}]$ (**9** (dppm), **14** (dppe)), and $[Fe_2(CO)_4(\mu\text{-}L\text{-}L)\{\mu\text{-}(CO)(CF_3)C_2(CF_3)S\}]$ (**10** (dppm), **15** (dppe)) has been observed from the reaction with 2 mol equiv of dppm or dppe. The product distribution is dependent on the reaction stoichiometry. Similar thermal reaction of 1 with 0.5 mol equiv of dppe gives quantitatively the dimeric cluster 11 $[\{Fe_2(CO)_5(\mu\text{-}(CF_3)C_2(CF_3)S)\}_2(\mu\text{-dppe})]$. Light-induced CO substitution in 1 leads to a mixture of tris- and tetrasubstituted products $[Fe_2(CO)_3L_3\{\mu\text{-}(CF_3)C_2(CF_3)S\}]$ (**5**) and $[Fe_2(CO)_2L_4\{\mu\text{-}(CF_3)C_2(CF_3)S\}]$ (**6**) (L = $P(OMe)_3$). Complexes **2**, **5**, **7**, **12**, **9**, and **14** were isolated as mixtures of two isomers which are in equilibrium. The molecular structures of compounds **2a**, **3a**, and **5** have been established by single-crystal X-ray diffraction studies. **2a** crystallizes in the monoclinic space group $P2_1/n$ with a = 7.584 (1) Å, b = 24.563 (4) Å, c = 11.028 (2) Å, β = 97.41 (2)°, R = 0.027 for 1709 reflections; **3a** crystallizes in the orthorhombic space group $P2_12_12_1$ with a = 10.646 (6) Å, b = 13.051 (4) Å, c = 18.258 (7) Å, R = 0.064 for 1129 reflections; **5** crystallizes in the triclinic space group $P\bar{1}$ with a = 9.447 (5) Å, b = 10.740 (1) Å, c = 16.205 (4) Å, α = 108.20 (1)°, β = 92.51 (3)°, γ = 110.22 (2)°, R = 0.036 for 2577 reflections. The three complexes have closely similar nido square pyramidal Fe_2–SC_2 skeletons. Electrochemical activation provides an alternative route to these substituted clusters and an efficient ETC-catalyzed substitution process of phosphine ligand for CO in 1 is described. Mechanisms proposed for these electrochemically induced substitutions are presented.

Introduction

The study of the reactivity of organic molecules linked to di- or polynuclear metal complexes has been of great interest for many years. Carbonyl substitution reactions in these derivatives have received particularly wide attention.[2] For these reactions, features of interest are (a) the stereochemistry of the products resulting on CO replacement by other nucleophile ligands and (b) preferential metal selectivity for CO substitution in asymmetric clusters. Electronic effects originating from both ligand and metal centers have been shown to influence the rate of dissociative CO loss and thus to determine the regio- and stereochemistry of the substitution reaction.[3] Substitution of CO ligands effected under thermal or photochemical conditions often leads to mixtures of mono- and polysubstituted derivatives, whereas the electrochemically induced reaction is highly stereoselective.[4] Efficient electron-transfer-chain (ETC) catalyzed substitution under reductive conditions requires that the substituted product must be harder to reduce than the parent complex:[2,4,5] this condition, which provides the driving force for the homogeneous electron transfer, is met when a π-acceptor (CO) is replaced by weaker π acids such as phosphites, phosphines, or diphosphines. Site-specific activity has been observed for various ligand substitutions in mixed-

(1) Part 8: Pétillon, F. Y.; Schollhammer, P.; Talarmin, J. *J. Organomet. Chem.* **1991**, *411*, 159.

(2) (a) Kochi, J. K. *J. Organomet. Chem.* **1986**, *300*, 139 and references cited therein. (b) Pétillon, F. Y.; Rumin, R.; Talarmin, J. *J. Organomet. Chem.* **1988**, *346*, 111 and references cited therein.

(3) (a) Shojaie, R.; Atwood, J. D. *Inorg. Chem.* **1987**, *26*, 2199 and references cited therein. (b) Don, M. J.; Richmond, M. G.; Watson, W. H.; Nagl, A. *J. Organomet. Chem.* **1989**, *372*, 417.

(4) (a) Savéant, J. M. *Acc. Chem. Res.* **1980**, *13*, 323. (b) Chanon, M.; Tobe, M. L. *Angew. Chem., Int. Ed. Engl.* **1982**, *21*, 1. (c) Astruc, D. *Angew. Chem., Int. Ed. Engl.* **1988**, *27*, 643.

(5) See for example: Richmond, M. G.; Kochi, J. K. *J. Organomet. Chem.* **1987**, *323*, 219 and references therein.

0276-7333/93/2312-0365$04.00/0

Table I. NMR Data for the Complexes (δ)[a]

complexes	^{19}F	$^{31}P^{b}$	$^{13}C^{b}$
1	–56.27 (q, 3 F, J_{FF} = 8.5) –61.90 (q, 3 F, J_{FF} = 8.5)		206.7 (s, 4 CO), 205.6 (s, CO), 203.0 (s, CO) [206.75 (s, CO), 206.6 (s, 3 CO), 205.5 (s, CO), 202.9 (s, CO)][c]
2a$_1$	–55.5 (dq, 3 F, J_{FF} = 8.5, J_{PF} = 2.6) –62.0 (dq, 3 F, J_{FF} = 8.5, J_{PF} = 1.2)	168.0 (qq, J_{PF} = 2.6, J'_{PF} = 1.2)	213.5 (d, J_{CP} = 29, CO), 210.5 (d, J_{CP} = 30.5, CO), 209.5 (s, CO), 209.2 (s, CO), 205.8 (s, CO), 136.5 (dq, J_{CF} = 39.5, J_{CP} = 6.5, C═CS), 125.8 (q, J_{CF} = 274, CF_3), 120.7 (q, J_{CF} = 275, CF_3), 103.35 (qq, J_{CF} = 43, J'_{CF} = 5, C═CS), 53.25 (d, J_{CP} = 6.5, $P(OMe)_3$)
2a$_2$	–55.05 (q, 3 F, J_{FF} = 8.5) –61.8 (dq, 3 F, J_{FF} = 8.5, J_{PF} = 1.5)	171.65 (q, J_{PF} = 1.5)	209.9 (d, J_{CP} = 26.5, CO), 209.7 (s, 3 CO), 206.8 (d, J_{CP} = 16, CO), 138.9 (dq, J_{CF} = 38.5, J_{CP} = 16, C═CS), 125.8 (q, J_{CF} = 275, CF_3), 120.7 (q, J_{CF} = 275, CF_3), 103.1 (qq, J_{CF} = 42, J'_{CF} = 3, C═CS), 53.0 (d, J_{CP} = 7, $P(OMe)_3$)
2b$_1$	–55.4 (q, 3 F, J_{FF} = 8.5) –59.2 (q, 3 F, J_{FF} = 8.5)	58.85 (s)	216.7 (d, J_{CP} = 15.5, CO), 214.5 (d, J_{CP} = 23, CO), 208.65 (s, CO), 207.4 (s, CO), 204.5 (s, CO), 135.6 (dq, J_{CF} = 39, J_{CP} = 6, C═CS), 134–128.5 (C_6H_5), 126.3 (q, J_{CF} = 274, CF_3), 120.5 (dq, J_{CF} = 276, J_{CP} = 2), 104.1 (ql, J_{CF} = 42, C═CS)
2b$_2$	–53.85 (m, 3 F) –60.05 (m, 3 F)	62.55 (s)	212.3 (l, CO), 209.5 (l, CO), 209.2 (s, 3 CO), 136–128.5 (C_6H_5, C═CS), 125.7 (q, J_{CF} = 275, CF_3), 120.25 (q, J_{CF} = 276, CF_3)
3a	–54.5 (dq, 3 F, J_{FF} = 8.5, J_{PF} = 3.3) –61.4 (dq, 3 F, J_{FF} = 8.5, J_{PF} = 2)	173.8 (q, 1 P, J_{PF} = 3.3) 176.85 (q, 1 P, J_{PF} = 2)	216.8 (dd, J_{CP} = 22.5, J'_{CP} = 3, CO), 213.2 (d, J_{CP} = 33, CO), 212.2 (d, J_{CP} = 24, CO), 208.2 (d, J_{CP} = 12.5, CO), 134.6 (ddq, J_{C-F} = 38, J_{CP} = 9, J'_{CP} = 14, C═CS), 126.6 (q, J_{CF} = 274, CF_3), 121.75 (q, J_{CF} = 274, CF_3), 101.05 (qq, J_{CF} = 41, J'_{CF} = 5, C═CS), 52.55 (d, J_{CP} = 5, $P(OMe)_3$), 52.45 (d, J_{CP} = 6, $P(OMe)_3$)
3b	–53.65 (q, 3 F, J_{FF} = 7.5) –56.8 (m, 3 F)	65.09 (s, 1 P)[d] 64.3 (s, 1 P)	220.45 (d, J_{CP} = 12, CO), 216.5 (d, J_{CP} = 25, CO), 213.9 (d, J_{CP} = 14.5, CO), 209.15 (d, J_{CP} = 9.5, CO), 135.4–128.2 (C_6H_5), 126.7 (q, J_{CF} = 276, CF_3), 120.9 (q, J_{CF} = 276, CF_3), 103.45 (ql, J_{CF} = 44, C═CS)
3c	–54.21 (dq, 3 F, J_{FF} = 8.5, J_{PF} = 3.0) –58.2 (dq, 3 F, J_{FF} = 8.5, J_{PF} = 1.5)	–19.9 (s, l, 1 P) –15.05 (s, l, 1 P)	
4a	–54.05 (dq, 3 F, J_{FF} = 8.5, J_{PF} = 3.4) –59.95 (dq, 3 F, J_{FF} = 8.5, J_{PF} = 1.6)	174.7 (s, l, 1 P) –14.65 (s, l, 1 P)	
4b	–54.55 (dq, 3 F, J_{FF} = 8.5, J_{PF} = 3.0) –59.25 (dq, 3 F, J_{FF} = 8.5, J_{PF} = 1.5)	177.7 (s, l, 1 P) –19.9 (s, l, 1 P)	
5a	–53.65 (ddq, 3 F, J_{FF} = 8.5, J_{PF} = 5.0, J_{PF} = 4.0) –60.15 ("tq", 3 F, J_{FF} = 8.5, J_{PF} = J'_{PF} = 1.5)	165.65 (ddq, 1 P, J_{PP} = 42.5, J'_{PP} = 9.5, J''_{PP} = 5.0) 178.0 (m, 1 P) 182.6 (dquin, 1 P, J_{PP} = 42.5, J'_{PP} = 1.8, J''_{PP} = 1.8)	219.3 (dd, J_{CP} = 19, J'_{CP} = 6, CO), 216.6 ("t", J_{CP} = 30, CO), 215.7 (d, J_{CP} = 37, CO)
5b	–54.1 (q, l, 3 F) –60.15 (m, 3 F)	173.95 (m, 1 P) 180.2 (m, 1 P) 180.3 (m, 1 P)	218.5 ("t", J_{CP} = 33, CO), 214.4 (d, J_{CP} = 27, CO), 209.7 (d, br, J_{CP} = 12, CO)
6	–53.0 (m, 3 F) –58.7 ("tq", 3 F, J_{PF} = 1.5)	167.9 (m, 1 P), 176.8 (m, 1 P) 178.4 (d, 1 P, J_{PP} = 7.5), 184.85 (ddhp, 1 P, J_{PP} = 42.5, J'_{PP} = 7.5, J_{PF} = J'_{PF} = 1.8)	221.15 (ddd, J_{CP} = 37, J'_{CP} = 19, J''_{CP} = 3, CO), 218.05 ("t", J_{CP} = 29, CO)
7a	–55.9 (dq, 3 F, J_{FF} = 8.5, J_{PF} = 1.8) –59.5 (ql, 3 F, J_{FF} = 8.5)	52.9 (d, l, 1 P, J_{PP} = 71.0) –25.7 (d, 1 P, J_{PP} = 71.0)	217.1 (d, J_{CP} = 14, CO), 214.05 (d, J_{CP} = 23.5, CO), 208.4 (s, CO), 207.7 (s, CO), 204.3 (s, CO), 137.7 (m, C═CS), 126.3 (q, J_{CF} = 274, CF_3), 121.2 (q, J_{CF} = 275, CF_3), 103.8 (qq, J_{CF} = 42.4, J'_{CF} = 5.5, C═CS), 32.5 (m, CH_2)
7b	–53.7 (q, 3 F, J_{FF} = 8.5) –60.45 (q, l, 3 F, J_{FF} = 8.5)	59.2 (d, l, 1 P, J_{PP} = 55.0) –25.9 (d, 1 P, J_{PP} = 55.0)	211.7 (d, J_{CP} = 14, CO), 209.6 (s, 3CO), 209.05 (d, J_{CP} = 10), 137.7 (m, C═CS), 126.2 (q, J_{CF} = 275, CF_3), 120.7 (q, J_{CF} = 275, CF_3), 103.8 (qq, J_{CF} = 42.5, J'_{CF} = 5.5, C═CS), 32.5 (m, CH_2)
8	–54.9 (dq, J_{FF} = 8.5, J_{PF} = 3.5) –62.3 (q, l, J_{FF} = 8.5)	47.5 (dq, 1 P, J_{PP} = 65.0, J_{PF} = 3.5) 56.0 (d, l, 1 P, J_{PP} = 65.0)	216.95 (d, J_{CP} = 21, CO), 214.9 (d, J_{CP} = 5, CO), 214.1 (d, J_{CP} = 22, CO), 207.35 (d, J_{CP} = 12, CO), 142.25 (q, br, J_{CF} = 30, C═CS), 141.75 (q, br, J_{CF} = 29.5, C═CS), 126.4 (q, J_{CF} = 274, CF_3), 121.1 (dq, J_{CF} = 276, J_{CP} = 3, CF_3), 49.2 (dd, J_{CP} = 22, J'_{CP} = 25.5, CH_2)
10	–52.45 (q, 3 F, J_{FF} = 10.0) –58.25 (q, l, 3 F, J_{FF} = 10.0)	50.55 (d, l, 1 P, J_{PP} = 79.0) 72.5 (d, l, 1 P, J_{PP} = 79.0)	239.7 (d, J_{CP} = 44.5, C(O)—C═C), 220.35 (d, J_{CP} = 16.5, CO), 215.3 (d, J_{CP} = 12, CO), 212.5 (d, J_{CP} = 10, CO), 207.8 (d, J_{CP} = 24.5, CO), 125.7 (q, J_{CF} = 276, CF_3), 122.5 (q, J_{CF} = 279, CF_3), 106.2 (dq, J_{CF} = 41.5, J_{CP} = 13.5, C═CS), 70.65 (m, C(O)C═CS), 41.6 (dd, J_{CP} = 27, J'_{CP} = 16.5, CH_2)
12a	–55.75 (dq, 3 F, J_{FF} = 8.5, J_{PF} = 1.6) –59.7 (q, l, 3 F, J_{FF} = 8.5)	55.35 (d, l, 1 P, J_{PP} = 37.0) –12.5 (d, 1 P, J_{PP} = 37.0)	217.1 (d, J_{CP} = 15, CO), 214.25 (d, J_{CP} = 23, CO), 208.5 (s, CO), 207.55 (s, CO), 204.25 (s, CO), 140.0 (dq, J_{CF} = 41, J_{CP} = 11, C═CS), 126.3 (q, J_{CF} = 274, CF_3), 121.0 (q, J_{CF} = 277, CF_3), 103.05 (dq, J_{CF} = 43, J_{CP} = 6.5, C═CS), 28.5 (m, CH_2), 22.5 (m, CH_2)
12b	–53.8 (q, 3 F, J_{FF} = 8.5) –60.65 (q, l, 3 F, J_{FF} = 8.5)	62.2 (d, l, 1 P, J_{PP} = 37.0) –12.7 (d, 1 P, J_{PP} = 37.0)	211.6 (d, J_{CP} = 16, CO), 209.7 (s, 3 CO), 208.85 (d, J_{CP} = 12, CO), 140.0 (dq, J_{CF} = 41, J_{CP} = 11, C═CS), 126.0 (q, J_{CF} = 275, CF_3), 120.6 (q, J_{CF} = 275, CF_3), 103.05 (dq, J_{CF} = 43, J_{CP} = 6.5, C═CS), 28.5 (m, CH_2), 22.5 (m, CH_2)

Table I. (Continued)

complexes	^{19}F	$^{31}P^b$	$^{13}C^b$
13	−53.95 ("tq", 3 F, J_{FF} = 8.5, J_{PF} = J'_{PF} = 2.2) −62.8 ("tq", 3 F, J_{FF} = 8.5, J_{PF} = J'_{PF} = 2.2)	52.4 (s, 1, 1 P) 67.8 (s, 1, 1 P)	215.6 (d, J_{CP} = 19, CO), 215.5 (d, J_{CP} = 9, CO), 213.85 (d, J_{CP} = 22.5, CO), 209.3 (d, J_{CP} = 17, CO), 126.15 (q, J_{CF} = 276, CF_3), 121.0 (dq, J_{CF} = 276, J_{CP} = 4.5, CF_3), 102.0 (m, C═CS), 30.2 (dd, J_{CP} = 29, J'_{CP} = 4, CH_2), 22.25 (d, J_{CP} = 21, CH_2)
14a	−55.1 ("tq", 3 F, J_{FF} = 8.0, J_{PF} = J'_{PF} = 1.8) −57.0 (dq, 3 F, J_{FF} = 8.0, J_{PF} = 3.0)	80.8 (d, 1, 1 P, J_{PP} = 4.0) 83.05 (d, 1, 1 P, J_{PP} = 5.0)	216.6 (dd, J_{CP} = 26.5, J'_{CP} = 14, CO), 209.9 (s, CO), 209.75 (s, 2 CO), 138.0 (m, C═CS), 97.5 (m, J_{CF} = 40, C═CS), 33.35 (AB, J_{CP} = 28.5, J'_{CP} = 14.5, CH_2), 29.7 (m, CH_2)
14b	−53.9 (dq, 3 F, J_{FF} = 8.5, J_{PF} = 3.2) −58.6 (dq, 3 F, J_{FF} = 8.5, J_{PF} = 1.2)	69.8 (dq, 1 P, J_{PP} = 9.0, J_{PF} = 3.2) 86.65 (d, 1, 1 P, J_{PP} = 9.0)	217.6 (dd, J_{CP} = 17, J'_{CP} = 19.5, CO), 217.1 (s, 3 CO), 138.0 (m, C═CS), 104.0 (m, J_{CF} = 42, C═CS), 30.3 (AB, J_{CP} = 27, J'_{CP} = 14, CH_2), 28.9 (AB, J_{CP} = 27, J'_{CP} = 11, CH_2)
15	−50.8 (q, 3 F, J_{FF} = 7.5) −58.35 (q, 3 F, J_{FF} = 7.5)	39.05 (d, 1 P, J_{PP} = 5.0) 63.35 (d, 1 P, J_{PP} = 5.0)	

[a] Chemical shifts (δ) in ppm measured in $CDCl_3$ at room temperature unless otherwise stated by *c* and *d*; *J* in Hertz. [b] Hydrogen-1 decoupled. [c] At −90 °C. [d] At −60 °C.

metal clusters;[5] rather less is known about homometallic compounds. With the aim of determining the sites occupied by successive incoming ligands, we have studied here the reaction of phosphite, phosphines, and diphosphines with $[Fe_2CO_6\{\mu\text{-}(CF_3)C_2(CF_3)S\}]$ (1), the synthesis and crystal structure of which we reported recently.[6] The presence in the complex of two dissimilar iron atoms at which ligand exchange can occur makes this cluster an ideal candidate for such a study. Herein we discuss the regioselectivity of nucleophilic CO substitution of this molecule under thermal, photochemical, and electrochemical activation.

Results

Thermal Reaction of $[Fe_2(CO)_6\{\mu\text{-}(CF_3)C_2(CF_3)S\}]$ with $P(OMe)_3$ and PPh_3. When 1 is heated with L = $P(OMe)_3$ or PPh_3 under reflux in tetrahydrofuran the mono- and disubstituted products $[Fe_2(CO)_5L\{\mu\text{-}(CF_3)C_2(CF_3)S\}]$ (2) (**2a**, L = $P(OMe)_3$; **2b**, L = PPh_3) and $[Fe_2(CO)_4L_2\{\mu\text{-}(CF_3)C_2(CF_3)S\}]$ (3) (**3a**, L = $P(OMe)_3$; **3b**, L = PPh_3) are obtained (Scheme I); when the mole ratio of L:1 is increased, at the start of the reaction production of the disubstituted product **3** is favored at the expense of **2**. The structures proposed for **2** and **3** in Scheme I are based on spectroscopic data (Table I) and X-ray diffraction studies (see below); they are derived from that of **1** by substitution of one or two CO ligands by $P(OMe)_3$ or PPh_3.

The ^{19}F, ^{31}P, and ^{13}C NMR data for **3a** indicate that this compound was obtained as a single structural isomer (Table I). The carbonyl region of the $^{13}C\{H\}$ NMR spectrum of **3a** contained four resonances, each split into a doublet by one adjacent cis phosphorous atom ($J_{C\text{-}P} \approx$ 22.5–33 Hz), thereby indicating that one CO/$P(OMe)_3$ substitution had occurred at each metal atom. X-ray analysis of **3a** confirms this conclusion: C(5)O on Fe(1) and C(9)O on Fe(2) in **1** are replaced by $P(OMe)_3$ in **3a** (see below). The assignment of the carbonyl resonances for **3a** was made by comparison of its ^{13}C NMR spectrum with that of the parent complex **1**. The room-temperature ^{13}C NMR spectrum of **1** contained three carbonyl signals in a 1:1:4 area ratio (Table I). At −90 °C, the area 4 signal had split into resonances at 206.75 ppm (area 1) and 206.6 ppm (area 3). Since four carbonyl resonances were observed, only localized scrambling of carbonyl groups at Fe(1) occurred at room temperature as well as at −90 °C. On the basis of X-ray structural data[6b] and by assuming that the Fe–C(O) distances in solution are comparable with those in the solid state, we tentatively assign the resonance (area 3) at 206.6 ppm to the three CO groups which are coordinated to the Fe(1) atom, the closely similar Fe(1)–C(O) distances (Table II) facilitating localized scrambling of the CO groups. The three singlets at 206.75, 205.5, and 202.9 ppm are then attributed to C(9)O [Fe(2)–C(9): 1.772 (5) Å], C(8)O [Fe(2)–C(8): 1.789 (5) Å], and C(10)O [Fe(2)–C(10): 1.834 (5) Å] (see Table II), respectively. Such an assignment is in agreement with that of Hickey et al.[7] for a cluster closely related to complex **1**. In comparison with **1**, the more shielded carbonyl ligand in the spectrum of **3a** is ascribed to the C(10)O group and

(6) (a) Rumin, R.; Pétillon, F. Y.; Manojlović-Muir, Lj.; Muir, K. W. *Organometallics* **1990**, *9*, 944. (b) Rumin, R.; Pétillon, F. Y.; Henderson, A. H.; Manojlović-Muir, Lj.; Muir, K. W. *J. Organomet. Chem.* **1987**, *336*, C50.

(7) Hickey, J. P.; Huffman, J. C.; Todd, L. J. *Inorg. Chim. Acta* **1978**, *28*, 77.

(8) Tolman, C. A. *Chem. Rev.* **1977**, *77*, 313.

Scheme I[a]

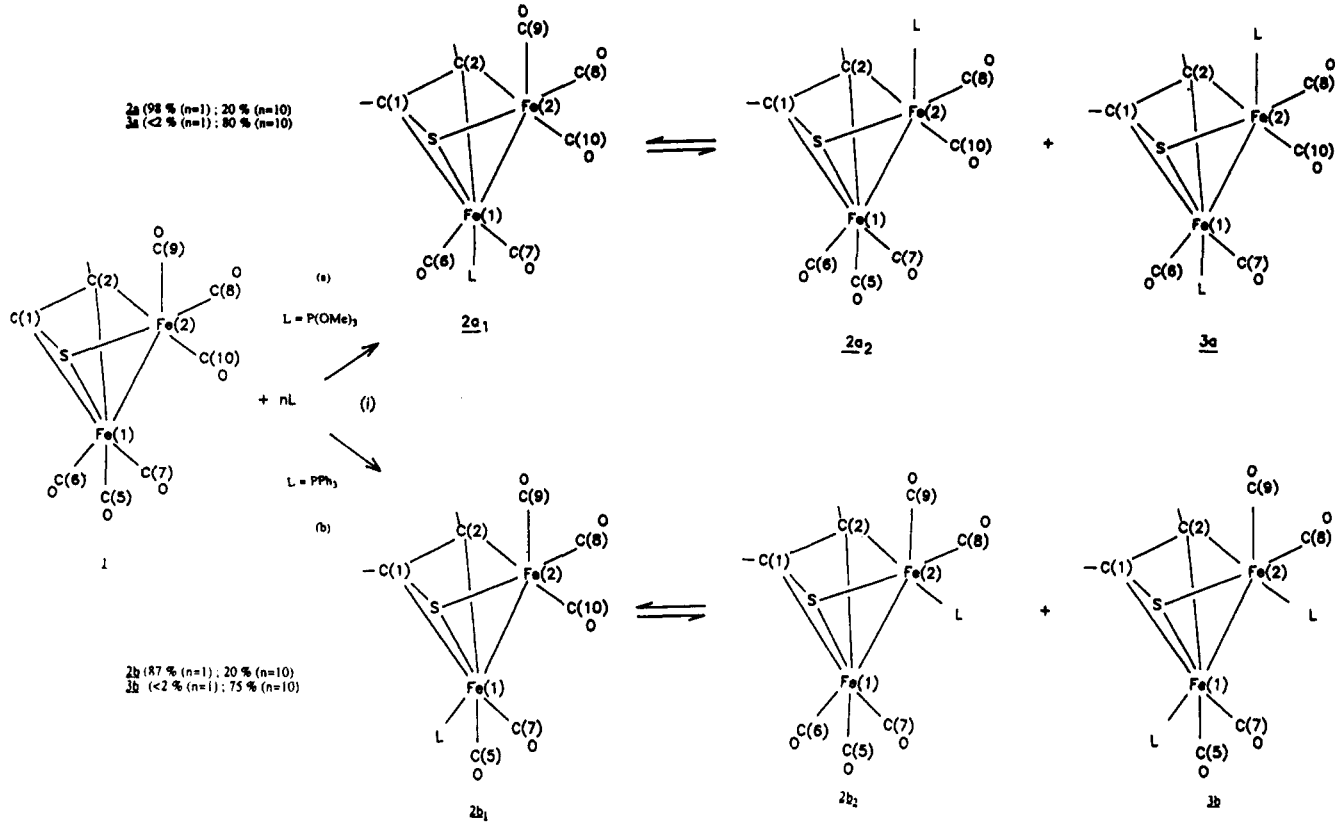

[a] Legend: (i) refluxed tetrahydrofuran, 17 H.

on the basis of the P(9)–carbon coupling, the higher field carbonyl resonance is assigned to the C(6)O group. The two resonances at 213.2 and 212.2 ppm are attributed to C(7) and C(8), but specific assignment is not possible.

NMR (^{19}F, ^{31}P, ^{13}C) spectrometry showed that compound **2** was isolated as a mixture of the isomers $\mathbf{2}_1$ and $\mathbf{2}_2$ (Scheme I). These were inseparable by conventional chromatographic techniques and were obtained in the same ratio from several preparations, suggesting strongly that they form an equilibrium mixture. Isomer $\mathbf{2a}_1$ can be isolated pure at low temperature (−90 °C, CD_2Cl_2 solution), and thermal isomerization leads to a mixture of $\mathbf{2a}_1$ and $\mathbf{2a}_2$. An X-ray structural determination has been made on crystals of $\mathbf{2a}_1$ (see below).

The coordination sites of the phosphite ligand in $\mathbf{2a}_1$ and $\mathbf{2a}_2$ have been determined on the basis of the $^{13}C\{^1H\}$ NMR spectra, as well as of the X-ray structural determination of the isomer $\mathbf{2a}_1$, and by comparison with **3a**. The ^{13}CO NMR spectrum of the mixture of $\mathbf{2a}_1$ and $\mathbf{2a}_2$ displayed two different patterns which can be unambiguously assigned by correlation with the parent **1** spectrum and from X-ray determinations. The pattern assigned to the most abundant isomer $\mathbf{2a}_1$ consisted of five signals of equal intensity, whereas that due to the less abundant isomer $\mathbf{2a}_2$ displayed two doublets ($J_{CP} \approx 21$ Hz) in addition to a singlet (see Table I) with an intensity ratio of 1:1:3. The two doublets in the $\mathbf{2a}_2$ pattern are attributable to two nonequivalent carbonyl groups which are bound to the iron atom (Fe(2)) bearing the phosphorus ligand; in comparison with **1** we ascribed the single resonance at 209.7 ppm to the three fluxional CO located on Fe(1). Given that the disubstituted compound **3a** derives from **1** by the replacement of the C(9)O group located on Fe(2) by a phosphite ligand, we suggest that $\mathbf{2a}_2$ is formed from **1** by replacement of C(9)O, as indicated in Scheme I. The ^{13}CO NMR pattern of $\mathbf{2a}_1$ is in accordance with the structure established by a single-crystal X-ray diffraction study (see below) which showed that C(5)O attached to Fe(1) in **1** is replaced by $P(OMe)_3$ in $\mathbf{2a}_1$. The low-field doublets ($J_{CP} \approx 30$ Hz) at 213.5 and 210.5 ppm are attributed to C(6)O [Fe(1)–C(6): 1.758 (7) Å] and C(7)O [Fe(1)–C(7): 1.765 (6) Å], and the three singlets at 209.5, 209.2, and 205.8 ppm are ascribed to C(8)O [Fe(2)–C(8): 1.768 (7) Å], C(9)O [Fe(2)–C(9): 1.775 (6) Å], and C(10)O [Fe(2)–C(10): 1.821 (6) Å], respectively. Comparison of the carbon–phosphorus coupling constants observed for **3a** ($J_{C(2)-P(5)} = 9$ Hz; $J_{C(2)-P(9)} = 14$ Hz), whose X-ray structure has been determined, with those of $\mathbf{2a}_1$ ($J_{C(2)-P(5)} = 6.5$ Hz) and $\mathbf{2a}_2$ ($J_{C(2)-P(9)} = 16$ Hz) is consistent with the assignment of isomers $\mathbf{2a}_1$ and $\mathbf{2a}_2$ indicated in Scheme I.

Isomers $\mathbf{2b}_1$ and $\mathbf{2b}_2$ have been characterized on the basis of their spectroscopic data. Comparison of their ^{13}C NMR patterns in the carbonyl region with those of $\mathbf{2a}_1$ and $\mathbf{2a}_2$ indicates unambiguously that the phosphine ligand is bound to two different iron atoms in $\mathbf{2b}_1$ and $\mathbf{2b}_2$, respectively. However the chemical shifts assigned to the **2b** carbonyl ligands are really different from those assigned to the **2a** CO, this suggests that the coordination sites of the phosphorus ligand in $\mathbf{2b}_1$ and $\mathbf{2b}_2$ differ from those determined in $\mathbf{2a}_1$ and $\mathbf{2a}_2$. The close similarity of the ^{13}C NMR patterns in the carbonyl region of $\mathbf{2b}_1$ and **7a** (dppm) or **12a** (dppe), and $\mathbf{2b}_2$ and **7b** or **12b** (see Table I and below) suggests that $\mathbf{2b}_1$ and $\mathbf{2b}_2$ are formed from **1** by replacement of C(6)O and C(10)O by a phosphine ligand, respectively. Spectroscopic data of **3b** are in agreement with the structure indicated in Scheme Ib.

Thermal Reactions of $[Fe_2(CO)_6\{\mu\text{-}(CF_3)C_2(CF_3)\text{-}S\}]$ (1) with Diphosphines. The diiron complex **1** reacted

Scheme II[a]

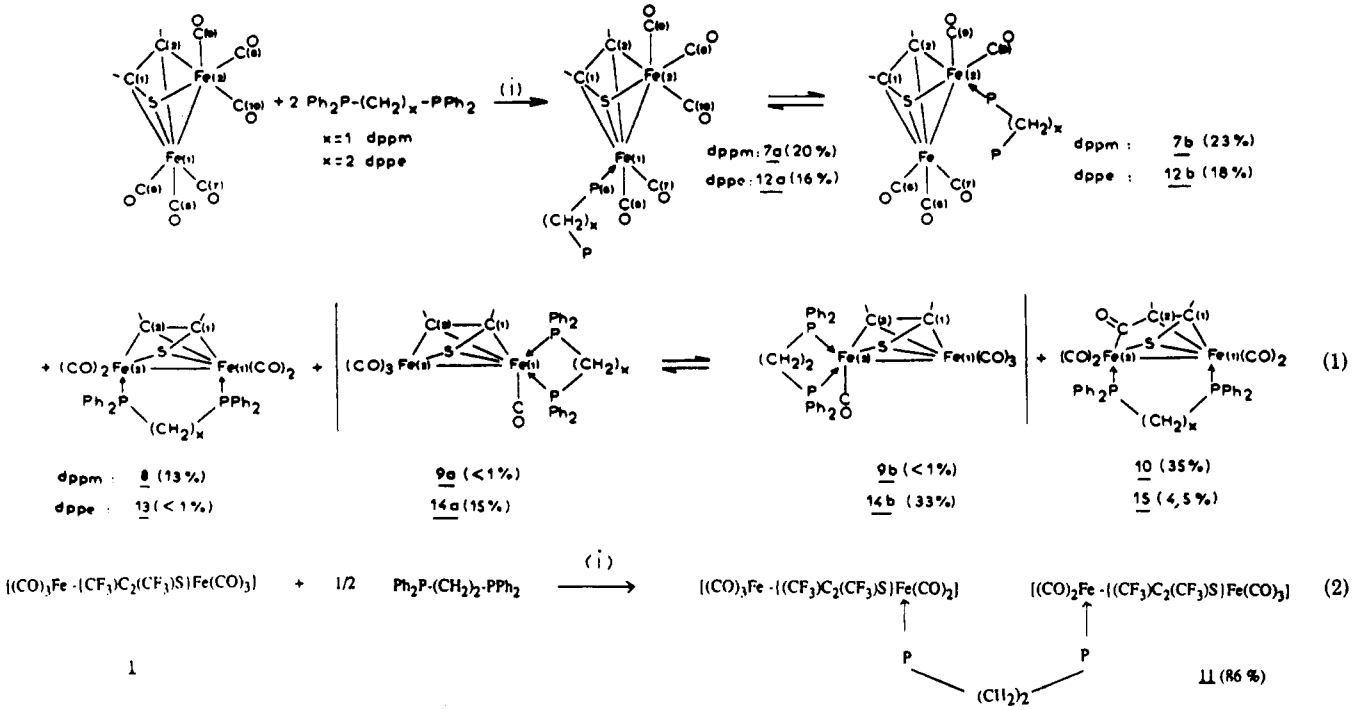

[a] Legend: (i) refluxed tetrahydrofuran, 17 H.

with 2 equiv of PPh_2–$(CH_2)_x$–PPh_2 (x = 1, dppm; x = 2, dppe) under reflux in tetrahydrofuran, affording a mixture of products (93% yield), which were separated by column chromatography. The nature of the products is not affected by the molar ratio of the reactants which again influences only the product distribution (see Scheme $II_{(1)}$): for example, when 1 equiv of dppm was used, increased yields (57%) of compound **7** were obtained.

As shown by mass spectrometry (see Experimental Section), two carbonyl groups of **1** have been readily displaced by one dppm or dppe ligand to form **8** or **13**, respectively. In the ^{13}CO NMR spectra, the presence of four doublets (J_{P-C} = 5–22 Hz) is accounted for if a diphosphine acts as a bridging bidentate ligand. In the $^{31}P\{^1H\}$ NMR spectra, the appearance of two resonances at low field is indicative of the inequivalence of the two P atoms. In these disubstituted compounds, there are nine possible isomers corresponding to the nine possible positions for the bridging bidentate ligand L-L. Compounds **8** and **13** were isolated as single isomers. Although their structures have not been definitively established we suggest that the bridging diphosphine replaces C(7)O and C(10)O in **1**: if the disubstituted complex **3a** is used as a model to estimate the P···P bite distances for the combinations P(x)–P(y) (x = 5–7; y = 8–10) (Figure 1), then the P(7)–P(10) bite distance is found to be ca. 3.5 Å, consistent with observed dppm and dppe bite distances of 3.0–3.5 Å in other complexes,[9] whereas all other P(x)–P(y) combinations lead to P···P separations of 3.85 Å or more.

The ^{13}CO NMR spectra of compound **10** showed (see Table I), in addition to the doublet at 239.7 ppm, a resonance pattern similar to those observed for the clusters **8** and **13**. This suggests that the dppm acts again as a bridging bidentate ligand in **10** and that it bridges the same sites as in **8** and **13**. The lower field resonance at 239.7 ppm, as well as the low wavenumber absorption in the IR spectrum at 1632 cm^{-1}, involved the formation of a CO-insertion product. The insertion of the carbonyl group in the Fe(2)–C(2) bond is indicated both by the large high-field shift of the resonance attributed to the C(2) atom in the ^{13}C NMR spectrum of **10** compared with that for the corresponding atom in **3a** (see Table I) and by the similar positions of the peaks assigned to C(1) in **10** and **3a**. In the mass spectrum successive loss of five carbonyl groups from the parent ion confirms the structure drawn for **10**. The close similarities of the solution IR and ^{19}F NMR spectra of **10** and **15** suggest that they both have the same structure.

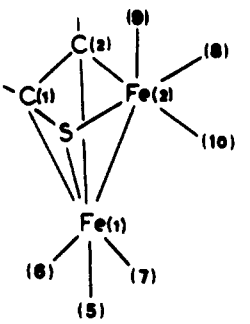

Figure 1. Possible isomeric positions of substitution in the clusters $[Fe_2(CO)_5L\{\mu\text{-}(CF_3)C_2(CF_3)S\}]$ (**2**).

The spectroscopic data (see Table I and Experimental Section) show that compounds **7** and **12** each exist in solution as a mixture of two isomers **a** and **b** which were inseparable by chromatography. The coordination mode of the dppm and dppe ligands in these clusters $[Fe_2(CO)_5(L\text{-}L)\{\mu\text{-}(CF_3)C_2(CF_3)S\}]$ (L-L = dppm, **7**; L-L = dppe, **12**) has been determined on the basis of $^{31}P\{^1H\}$ NMR and

(9) (a) Don, M. J.; Richmond, M. G.; Watson, W. H.; Kashyap, R. P. *Acta Crystallogr.* **1991**, *C47*, 20. (b) Churchill, M. R.; Lashewycz, R. A.; Shapley, J. R.; Richter, S. I. *Inorg. Chem.* **1980**, *19*, 1277. (c) Wright, M. E.; Mezza, T. M.; Nelson, G. O.; Armstrong, N. R.; Day, U. W.; Thompson, M. R. *Organometallics* **1983**, *2*, 1711. (d) Palenik, G. J.; Mathew, M.; Steffen, W. L.; Beran, G. *J. Am. Chem. Soc.* **1975**, *97*, 1059. (e) Braunstein, P.; Richert, J. L.; Dusausoy, Y. *J. Chem. Soc., Dalton Trans.* **1990**, 3804.

Scheme III[a]

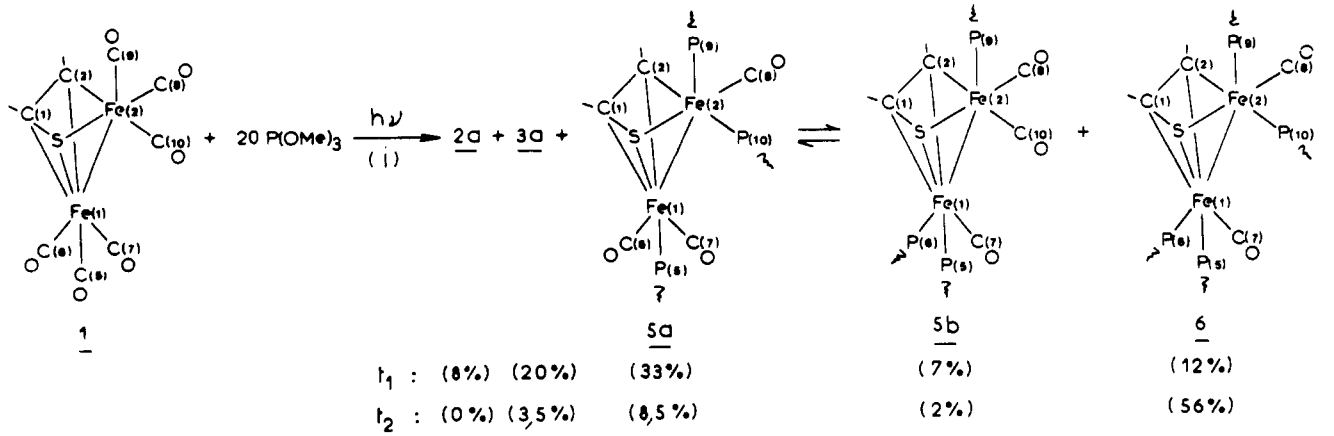

[a] Legend: (i) room temperature, tetrahydrofuran, t_1 = 15 min, t_2 = 90 min.

mass spectrometry. In the ^{31}P NMR spectra of each isomer **a** or **b**, the presence of two resonances is indicative of the inequivalence of the two P atoms. The higher field resonances at ca. −25.7 ppm (dppm complexes) and −12.5 ppm (dppe complexes) are almost unshifted from the signal of the free phosphine,[8] which indicates that the diphosphine is bound in a unidentate manner. This is confirmed by the mass spectra which show parent-ion peaks at m/z 830 and 844 (^{56}Fe) for **7** and **12**, respectively. The ^{13}CO NMR patterns of complexes **7a,b** and **12a,b** are roughly similar to those of **2a**$_1$,**a**$_2$, which confirms that the dppm and the dppe act as monodentate ligands in **7** and **12**. However, appreciable change is observed with respect to their respective chemical shifts, suggesting strongly that the carbonyl ligands which are replaced at Fe(1) (isomers **a**) and Fe(2) (isomers **b**) in **1** to form **7** and **12** are not C(5)O and C(9)O as is the case in the formation of **2a**$_1$,**a**$_2$. The structures assigned to **7** and **12** in Scheme II are based on the consideration that in **1** C(6)O and C(10)O are the least sterically hindered sites on Fe(1) and Fe(2); they are also consistent with the observation that when a mixture of **7a,b** is refluxed in toluene, it transforms into **10** in which the dppm ligand replaces the C(10)O carbonyl.

Complexes **9** and **14** were isolated as a mixture of two isomers **a,b**. In those compounds, the bidentate ligands chelate either the Fe(1) atom (**a**) or the Fe(2) atom (**b**) of the species depicted in Scheme II$_{(1)}$. Supporting evidence for the chelating behavior comes from the large downfield shifts exhibited by **14** in the ^{31}P NMR spectra (see Table I) which must be a consequence of the formation of five-membered chelate rings.[10] The ^{13}CO NMR spectrum of **14a** showed a doublet of doublets at 216.6 ppm and two singlets at 209.9 and 209.75 ppm, in the intensity ratio 1:1:2, as required for the suggested structure. Similarly, the ^{13}CO resonance pattern of **14b**, consisting of a doublet of doublets at 217.6 and a singlet at 217.1 ppm in the intensity ratio 1:3, is in accordance with the structure depicted in Scheme II$_{(1)}$. For both isomers **14a** and **14b**, the highest frequency resonance is easily assigned to the single CO at Fe(1) (**a**) or at Fe(2) (**b**). We observed again that the three CO located on Fe(1) gave a single resonance in **14b**, which indicates rapid intramolecular exchange of these carbonyl groups at room temperature. In both compounds **14a** and **14b** there are three possible isomeric forms corresponding to the three possible positions for the chelating ligand dppe at Fe(1) or Fe(2). For each compound, only one isomer is observed in solution. In view of steric hindrance, and by analogy with compounds **5** and **6** (see below), we favor the "P(5)–P(6)" and the "P(9)–P(10)" isomeric forms in **14a** and **14b**, respectively. Complexes **9** and **14** exhibited very similar behavior (e.g., ^{19}F NMR pattern: minor product **9a** [−57.3 (m), −54.9 (m)], major product **9b** [−59.4 (dq), −53.9 (q, br)]).

The dimeric cluster [(Fe$_2$(CO)$_5${μ-(CF$_3$)C$_2$(CF$_3$)S})$_2$(μ-dppe)] (**11**) (Scheme II$_{(2)}$) has been characterized by IR mass, ^{19}F, ^{31}P, and ^{13}C NMR spectrometry. The mass spectrum unambiguously showed a parent-ion peak at m/z 1290, which is consistent with its proposed formulation. In addition, the IR solution spectrum of **11** in the carbonyl region (see Experimental Section) closely resembles that of the monosubstituted derivative **12** and the only way to maintain the same carbonyl geometry is by having the dppe ligand linking two cluster units. The ^{31}P NMR spectrum confirms the absence of a pendant mode for the dppe ligand. The ^{19}F and ^{13}C NMR spectra of **11** closely resemble those of compounds **7** and **12**. The ^{19}F NMR spectrum showed clearly the presence in solution of at least three isomers; these could not be separated, nor their structures determined.

Photolytic Reaction of [Fe$_2$(CO)$_6${μ-(CF$_3$)C$_2$(CF$_3$)S}] Cluster 1 with Trimethyl Phosphite. Photolytic displacement of CO ligands from **1** in the presence of a large excess of P(OMe)$_3$ (20 equiv) gives a mixture of mono- (**2a**), di- (**3a**), tri- (**5**), and tetrasubstituted (**6**) products which were separated by column chromatography. The nature of the products, as well as the product distribution, depends on the photolysis time. Spectroscopic data given in Table I are consistent with the structures drawn for **5** and **6** (Scheme III).

In the trisubstituted cluster **5** there are 18 possible isomers corresponding to the distribution of three monodentate ligands L over two inequivalent iron atoms. NMR spectrometry shows that **5** was isolated as a mixture of two isomers **5a,b**, which were inseparable by chromatography. The coordination sites of the three phosphite ligands in **5a** and **5b** have been determined on the basis of their $^{13}C\{^1H\}$ NMR spectrometry and of the X-ray structural determination of **5a** (see below). In **5a**, the phosphite ligands occupy axial positions at Fe(1) [P(5)] and at Fe(2) [P(9)] and an equatorial position at Fe(2) [P(10)] (see molecular structure section). The ^{13}C NMR of **5a** shows the expected triplet and two doublets (Table

(10) Grim, S. O.; Briggs, W. L.; Barth, R. C.; Tolman, C. A.; Jesson, J. P. *Inorg. Chem.* **1974**, *13*, 1095.

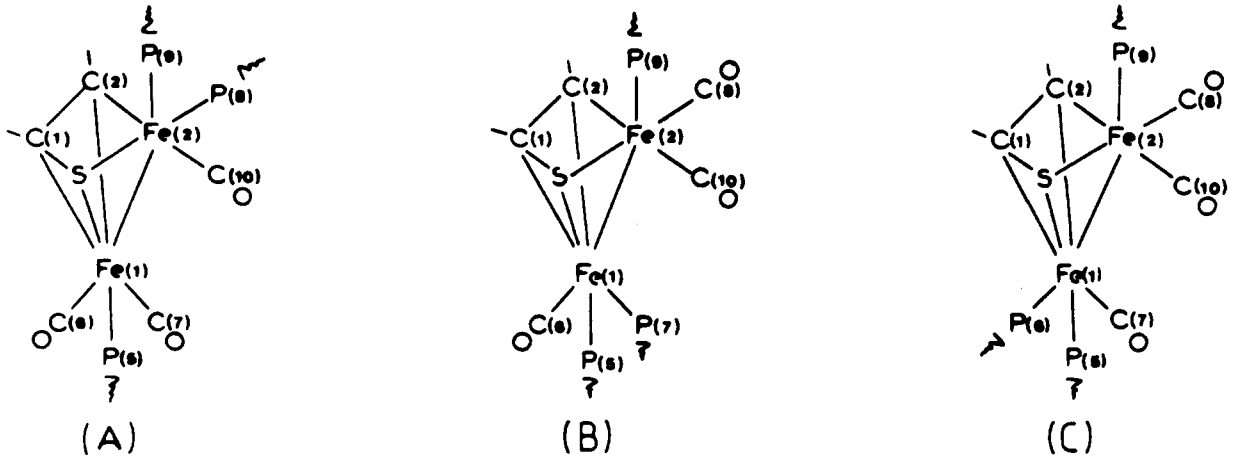

Figure 2. Possible isomeric configurations in the tris-substituted cluster $[Fe_2(CO)_3L_3\{\mu\text{-}(CF_3)C_2(CF_3)S\}]$ (**5b**).

I) in the intensity ratio 1:1:1. The triplet at 216.0 ppm (J_{P-C} = 30 Hz) is easily assigned to the unique equatorial C(8)O at Fe(2) whereas the equatorial C(6)O and C(7)O at Fe(1) are responsible for the two doublets. The nature of the less abundant isomer **5b** present in solution is not completely clear, but of the possible isomers those which do not contain the phosphine P atoms in both axial positions (P(5) and P(9)) can be ruled out on the basis of the systematic occupancy of these sites in compounds **2a**, **3a**, and **5a** whose structures have been ascertained by an X-ray determination. Thus, for **5b** three possible structures can be proposed, A–C in Figure 2. The ^{13}C NMR spectrum of **5b** shows a triplet at 218.5 ppm and two doublets at 214.4 and 209.7 ppm in the intensity ratio 1:1:1. The triplet is clearly due to the single carbonyl remaining at the iron atom which bonds two phosphorus ligands, and the two other resonances are assigned to the two CO located on the second iron atom. We noticed in the range of compounds studied here (see Table II)that the presence of one or two phosphine P atoms at an iron atom decreases the length of the remaining Fe–C(O) bonds by 0.03–0.05 Å compared with Fe–C(O) distances in the unsubstituted species. On the basis of these data, we calculated the average Fe–C(O) distances in the three possible configurations (A–C) for compound **5b**. If a correlation between Fe–C(O) distances and ^{13}CO NMR shifts is assumed, B and C are in accord with the ^{13}CO NMR pattern of **5b** but A is not; C is less sterically hindered than B.

The photoinduced displacement of four CO ligands from 1 led to the formation of complex **6** which is the major product of the reaction after a prolonged time of photolysis (90 min). The structure of **6** is readily deducible from NMR (^{19}F, ^{31}P, ^{19}C) spectrometry: a single isomer was obtained (see Table I); its ^{13}C NMR spectra displays in the carbonyl region a doublet of doublets of doublets at 221.15 ppm and a pseudotriplet at 218.05 ppm, in the intensity ratio 1:1 in accordance with the suggested structure. We assume that the CO substitution by $P(OMe)_3$ at Fe(1) and at Fe(2) occurred at the less sterically hindered positions which suggests that the two remaining carbonyl groups in **6** are C(8)O at Fe(2) and C(7)O at Fe(1).

Structural Characterization of Compounds $2a_1$, $3a_1$, and $5a_1$. The structures of the products of stepwise replacement of three of the carbonyl ligands in $[Fe_2(CO)_6\{\mu\text{-}(CF_3)C_2(CF_3)S\}]$ (1) by $P(OMe)_3$ have been established by single diffraction analysis of $[Fe_2(CO)_{6-n}\{P(OMe)_3\}_n\{\mu\text{-}(CF_3)C_2(CF_3)S\}]$, n = 1 ($2a_1$), 2 (**3a**), and 3 (**5a**) (see Figures 3–5 and Table II). Although the first carbonyl to be replaced is attached to Fe(1), the second and third substitutions both involve Fe(2).

Table II. Principal Bond Lengths (Å) in the Complexes $[Fe_2(CO)_{6-n}\{P(OMe)_3\}_n\{\mu\text{-}(CF_3)C_2(CF_3)S\}]$, Where n = 0–3[a]

n =	0	1	2	3
L^1 =	CO	$P(OMe)_3$	$P(OMe)_3$	$P(OMe)_3$
L^2 =	CO	CO	$P(OMe)_3$	$P(OMe)_3$
L^3 =	CO	CO	CO	$P(OMe)_3$
Fe–Fe	2.533 (1)	2.523 (1)	2.535 (4)	2.570 (1)
Fe(1)–S	2.260 (2)	2.256 (2)	2.267 (7)	2.267 (2)
Fe(1)–C(1)	2.027 (4)	2.039 (5)	1.97 (2)	2.010 (6)
Fe(1)–C(2)	2.080 (4)	2.056 (5)	2.05 (2)	2.090 (6)
Fe(1)–L^1	1.803 (4)	2.170 (2)	2.166 (6)	2.166 (2)
Fe(1)–C(6)	1.790 (4)	1.758 (7)	1.70 (3)	1.760 (6)
Fe(1)–C(7)	1.799 (4)	1.765 (6)	1.70 (3)	1.772 (7)
Fe(2)–S	2.273 (2)	2.271 (2)	2.290 (7)	2.272 (2)
Fe(2)–C(2)	1.935 (4)	1.939 (5)	1.95 (2)	1.942 (6)
Fe(2)–C(8)	1.789 (5)	1.768 (7)	1.70 (2)	1.742 (6)
Fe(2)–L^2	1.772 (5)	1.775 (6)	2.158 (7)	2.120 (2)
Fe(2)–L^3	1.834 (5)	1.821 (6)	1.71 (4)	2.195 (2)
C(1)–C(2)	1.406 (5)	1.400 (7)	1.37 (3)	1.416 (8)
C(1)–S	1.752 (4)	1.742 (5)	1.77 (2)	1.763 (6)

[a] The atom numbering scheme is

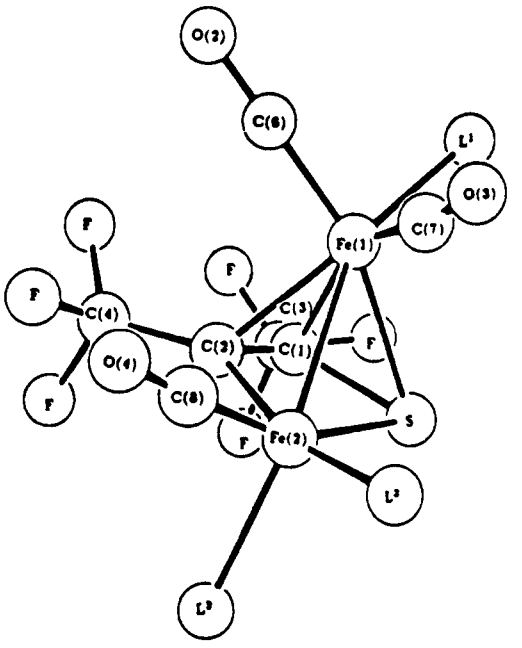

Structural details for the three complexes $2a_1$, **3a**, and **5a** are presented in Table II, together with corresponding values from our previous analysis of the starting (n = 0)

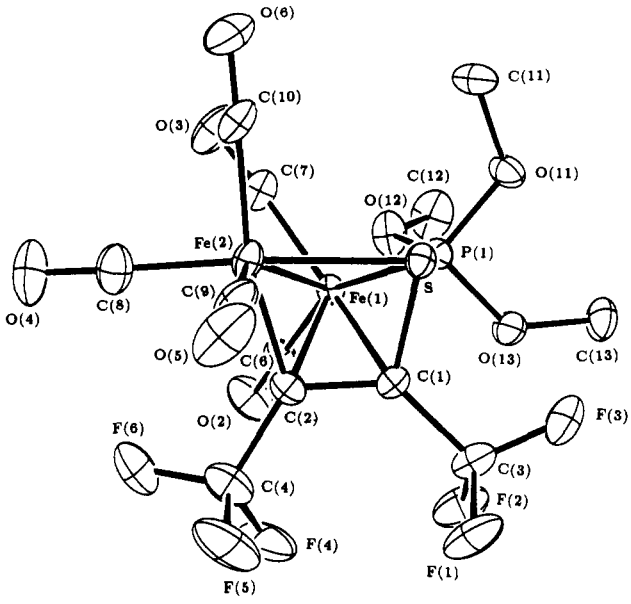

Figure 3. View of the structure of $[Fe_2(CO)_5\{P(OMe)_3\}\{\mu\text{-}(CF_3)C_2(CF_3)S\}]$ ($\mathbf{2a}_1$). Here and in Figures 4 and 5 hydrogen atoms are omitted and other atoms are represented by 20% probability ellipsoids.

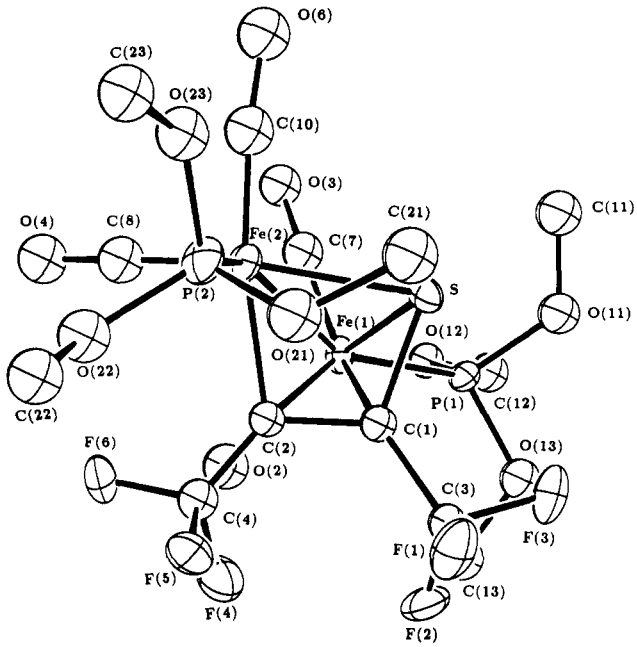

Figure 4. View of the structure of $[Fe_2(CO)_4\{P(OMe)_3\}_2\{\mu\text{-}(CF_3)C_2(CF_3)S\}]$ (**3a**). The disorder of methyl carbons C(21) and C(23) is not shown.

complex 1.[6b] In considering Table II the lower accuracy of the results for the $n = 2$ complex **3a** should be bourne in mind. The atom numbering scheme used here for all four complexes is also explained in Table II. The complexes have closely similar nido square pyramidal Fe_2C_2S skeletons, as expected for five-atom clusters with seven skeletal electron pairs (one from each Fe atom, two from S and 1.5 from each C atom). Fe(1) occupies the apex of the pyramid and is bonded to all four basal atoms. The stereochemistry at Fe(1) is essentially the same in all four structures: corresponding valency angles at Fe(1) agree well, the largest variation being shown by the C(2)–Fe(1)–L^1 angle which increases from 132° when $n = 0$ and L = CO (1) to 141–148° in the other complexes where L = $P(OMe)_3$. The stereochemistry at Fe(2) shows even less

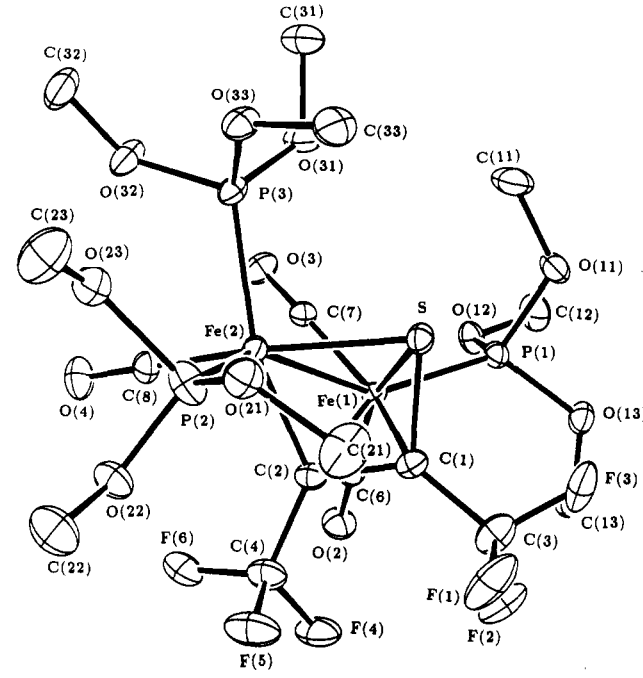

Figure 5. View of the structure of $[Fe_2(CO)_3\{P(OMe)_3\}_3\{\mu\text{-}(CF_3)C_2(CF_3)S\}]$ (**5a**). The disorder of O(21) and O(23) is not shown.

dependence on the pattern of substitution: corresponding valency angles agree to within 4°. Each Fe atom carries three carbonyl or phosphite ligands which subtend angles of 89–99° at the metal atom. Fe(1) thus has a coordination number of 7, compared with 6 for Fe(2).

Bond lengths in all four structures agree well with recently compiled average values[11] from the Cambridge Structural Database such as, for example, Fe–CO = 1.782 (30), Fe–$P(OMe)_3$ = 2.151 (17), and Fe(μ_3-S) = 2.281 (35) Å. The small variations between structures apparent from Table II can mostly be related to expected electronic effects. For example, the lower π-acidity of phosphite compared with carbonyl accords with the observation that replacement of CO by $P(OMe)_3$ is accompanied by a shortening of the remaining Fe–CO bonds at the same metal by ca. 0.03 Å (e.g., compare the Fe(1)–CO distances when $n = 0$ (1) with those in the $n = 1$ ($\mathbf{2a}_1$) and $n = 3$ (**5a**) complexes). Likewise, the higher trans influence of σ-C relative to Fe is reflected in a lengthening of Fe(2)–L^3 relative to Fe(2)–L^2 by 0.05–0.08 Å both when $L^2 = L^3$ = CO ($n = 0$ or 1) and when $L^2 = L^3 = P(OMe)_3$ ($n = 3$). Finally, we note the consistent variation in the Fe–CCF_3 distances: Fe(1)–C(2) > Fe(1)–C(1) > Fe(2)–C(2), with the Fe(2)–C(2) bonds appearing short compared with the mean length of 2.006 (45) Å[11] for a σ-Fe–C sp^2 bond.

It is obvious from the discussion of Scheme I that the factors which determine whether monosubstitution occurs on Fe(1) or Fe(2) are rather finely balanced, though $\mathbf{2a}_1$, the thermodynamic product, carries phosphite on Fe(1), the metal atom with the higher coordination number. However, replacement of CO by $P(OMe)_3$ at Fe(1) strengthens the remaining Fe(1)–CO bonds and increases steric congestion at Fe(1); both these factors disfavor further substitution at Fe(1). Furthermore, it is apparent from Figures 3–5 that approach to the C(8)–O(4) carbonyl

(11) (a) Orpen, A. G.; Brammer, L.; Allen, F. H.; Kennard, O.; Watson, D. G.; Taylor, R. *J. Chem. Soc., Dalton Trans.* **1989**, S1. (b) Allen, F. H.; Kennard, O.; Watson, D. G.; Brammer, L.; Orpen, A. G.; Taylor, R. *J. Chem. Soc., Perkin Trans. 2* **1987**, S1.

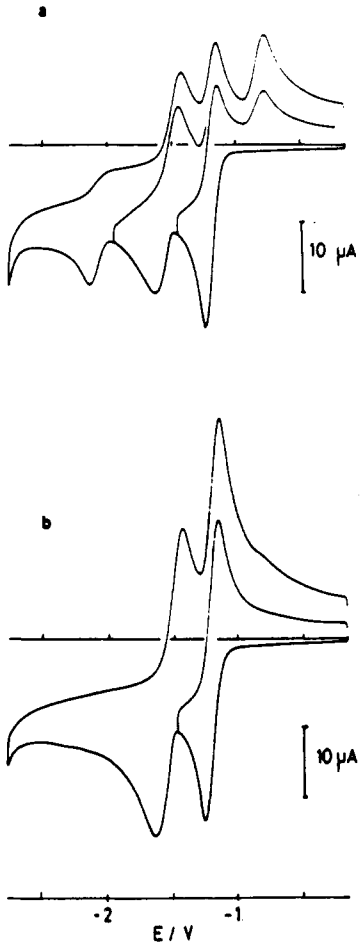

Figure 6. Cyclic voltammograms of a 0.9 mM solution of 1 (a) under N_2 and (b) under CO in THF–$[Bu_4N][PF_6]$ (vitreous carbon electrode; v = 0.2 V·s^{-1}).

attached to Fe(2) is partially blocked by the trifluoromethyl substituent on C(2) and by carbonyls on Fe(1) so that further substitutions at Fe(2) occur at the less sterically hindered L^2 and L^3 positions.

Electrochemical Studies. Electrochemical Behavior of 1 in the Absence of Phosphine Ligands. The cyclic voltammetry (CV)[12] of complex 1 in a THF–$[Bu_4N][PF_6]$ electrolyte under an inert atmosphere (Figure 6a) displays three reduction steps, with the first two quasi-reversible. The primary reduction at $E^{1/2}$ = −1.19 V is a one-electron process (n = 0.95 ± 0.05 by coulometry). The scan rate dependence of $\Delta E_{p\ red1}$ (ΔE_p increases from 90 mV at 0.02 V·s^{-1} to 190 mV at 1 V·s^{-1}) and of $(i_p^a/i_p^c)_{red1}$ (i_p^a/i_p^c increases from 0.45 at 0.02 V·s^{-1} to 0.90 at 1 V·s^{-1}) indicates that the heterogeneous electron transfer is not fully reversible and that a chemical step is coupled to the electron transfer at $E_{p\ red1}$.[13] The nature of the chemical reaction will be discussed in more detail below. The fact that the second reduction at $E^{1/2}$ = −1.56 V involves the radical anion generated at $E_{p\ red1}$ is demonstrated by the increase of $i_p^{c}{}_{red2}/i_p^{c}{}_{red1}$ on increasing v, a condition which also improves the chemical reversibility of the primary reduction. The second reduction process is even less

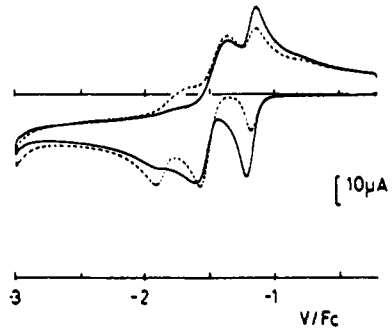

Figure 7. Cyclic voltammograms of a 0.9 mM solution of 1 in the presence of 1 equiv of $P(OMe)_3$ (- - -) under N_2 and (—) under CO in THF–$[Bu_4N][PF_6]$ (vitreous carbon electrode; v = 0.2 V·s^{-1}).

Scheme IV. Reduction Mechanism of Complex 1 at Room Temperature under N_2 in a THF Electrolyte

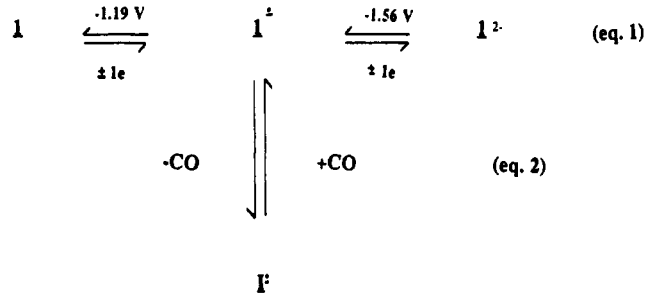

reversible than the first one with $(i_p^a/i_p^c)_{red2} < 1$ and $\Delta E_p \gg 60$ mV (Figure 6a). The third irreversible reduction ($E_{p\ red}$ = −2.17 V) and the irreversible oxidation at $E_{p\ ox}$ = −0.75 V are due to a product ($I^{\bullet-}$) generated by the EC process at $E_{p\ red1}$ (Figure 6a, Scheme IV).

The dramatic change observed when the CV of 1 is run under a CO atmosphere (Figure 6b) is very informative as to the nature of the chemical reaction coupled to the primary reduction. This step becomes chemically reversible [$(i_p^a/i_p^c)_{red1}$ = 1] in the presence of CO, whereas the irreversible peaks associated with $I^{\bullet-}$ are completely suppressed. The increased stability of $1^{\bullet-}$ in the presence of CO is further confirmed by the enhancement of the second reduction peak current (Figure 6b). These facts demonstrate unambiguously that the chemical reaction coupled to the primary electron transfer consists of the reversible loss of a carbonyl from $1^{\bullet-}$ (see Scheme IV, step 2).

Electrosynthesis of Singly Substituted Derivatives of 1. The presence of a 17-electron metal center in the electrogenerated $I^{\bullet-}$ (Scheme IV) suggests that 1 should readily undergo the substitution of donor ligands for CO according to a reductively initiated ETC-catalyzed process.[12,14] That it is indeed the case is demonstrated by the CV of 1 run in the presence of 1 equiv of $P(OMe)_3$ (Figure 7, dashed line): under these conditions the primary reduction of 1 is severely suppressed and the redox processes associated with $I^{\bullet-}$ are wiped out. The quasi-reversible couple around −1.5 V is due to the monosubstituted derivative **2a**, formed during the CV scan. Whereas the substitution is retarded by CO (Figure 7, solid line), an increase in the ratio $[P(OMe)_3]/[1]$ results in a further suppression of the primary reduction step and in shorter reaction time and lower charge consumption

(12) Abbreviations in electrochemical part: CV, cyclic voltammetry; cpe, controlled potential electrolysis; n, number of electrons; i_p^a and i_p^c, anodic and cathodic peak current; v, scan rate; E_p^a and E_p^c, anodic and cathodic peak potential, $\Delta E_p = [E_p^a - E_p^c]$; $E^{1/2} = (E_p^a + E_p^c)/2$; an EC process consists of an electron-transfer step (E) followed by a chemical reaction (C); ETC, electron transfer chain.

(13) Bard, A. J.; Faulkner, L. R. *Electrochemical Methods. Fundamentals and Applications*; Wiley: New-York, 1980.

(14) For reviews dealing with ETC catalysis see refs 2a and 4.

Table III. Electrosynthesis of Substituted Derivatives of 1

entry	mol of complex 1	ligand (no. of equiv)	E applied (V/Fc)	charge consumed (F/mol of 1)	reaction time (s)	products (yield)
1	4×10^{-4}	$P(OMe)_3$ (1)	−1.2	0.01	120	**2a** (89)[a]
2	1.8×10^{-4}	$P(OMe)_3$ (1)	−1.2	0.008	80	**2a** (100)[b]
			−1.6	0.003	250	**3a** (90)[a]
3	1.1×10^{-4}	dppm (1)	−1.2	0.02	200	**7** (67)[a]
			−1.5	0.13	600	**8** (47)[a]
						10 (35)[a]
4	3×10^{-5}	dppe (0.5)	−1.2	0.02	175	**11** (84)[a]
5	3.2×10^{-4}	dppe (1)	−1.2	0.008	50	**12** (79)[a]
			−1.6	0.096	500	**13** (68)[a]
						14 (10)[a]

[a] Yield after extraction and column chromatography. [b] Yield estimated from CV peak currents, assuming identical diffusion coefficients for reactant and product.

Table IV. Redox Potentials of Complex 1 and of Its Substituted Derivatives[a]

ligand	complex	primary reduction $E^{1/2}$ (V/Fc)	other processes
	1	−1.19	−1.56 ($E^{1/2}_{red2}$)
$P(OMe)_3$	**2a**	−1.51	−1.98 (E_p)
	3a	−1.88[b]	−2.3
dppm	**7**	−1.48	−1.86, −2.10
	8	−1.88	−2.2
	10	−1.56	−1.87, −2.3
dppe	**11**	−1.55 (E_p)	−1.87, −2.2
	12	−1.47	−1.88, −2.2
	13	−1.88	−2.2
	14	−1.87	−2.2
	15	−1.53	−2.2

[a] CV measurements in THF $[Bu_4N][PF_6]$; scan rate 0.2 V·s^{-1}. [b] Reversible at 0 °C or in the presence of $P(OMe)_3$.

during the electrolyses (Table III, entries 1 and 2). This is consistent with the dissociative nature of the substitution process (reactions 1 and 2), and with the rate law expressed by eq 3.[15]

$$1^{\bullet-} \underset{k_{-1}}{\overset{k_1}{\rightleftharpoons}} (I^{\bullet-}) + CO \qquad (1)$$

$$(I^{\bullet-}) + P(OMe)_3 \xrightarrow{k_2} \mathbf{2a}^{\bullet-} \qquad (2)$$

$$-\frac{d[1^{\bullet-}]}{dt} = \frac{k_1 k_2 [1^{\bullet-}][P(OMe)_3]}{k_{-1}[CO] + k_2[P(OMe)_3]} \qquad (3)$$

Cpe performed at the potential of the primary reduction of 1 in the presence of a phosphorus ligand affords, by selective and very rapid means and with a low charge consumed, the singly substituted derivatives (**2a**, **7**, or **12**) as the same equilibrium mixture of two isomers also obtained by a thermal route. These singly substituted compounds, identified by comparison of their spectra (IR, ^{19}F and ^{31}P NMR) with those of authentic samples are characterized by a quasi-reversible reduction whose potential (ca. −1.5 V) is almost independent of the nature of the substituting phosphorus ligand (see Table IV). Other redox processes, which can be assigned to the disubstituted compounds, are also observed on the CV scans and will be detailed below.

In conclusion, the reduction of 1 in the presence of $^1/_2$ equiv of dppe leads to the formation of **11** (Table III, entry 4).

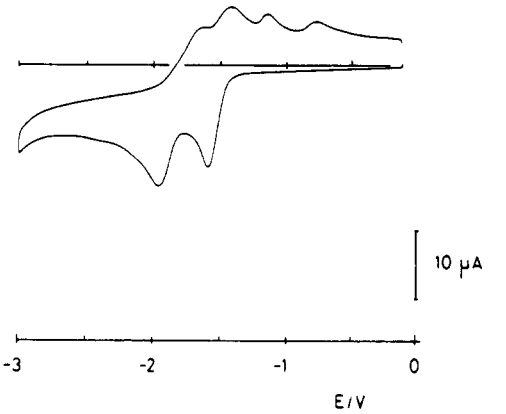

Figure 8. Cyclic voltammogram of a 0.7 mM solution of **2a** at room temperature under N_2 (vitreous carbon electrode; v = 0.2 V·s^{-1}).

Electrochemistry of Complex 2a in the Absence of Phosphorus Ligand. Complex **2a** undergoes two reduction steps in the potential domain ranging from 0 to −3.0 V in THF–$[Bu_4N][PF_6]$ (Figure 8). The analysis of the scan rate dependence of various electrochemical parameters $[(i_p^a/i_p^c)_{red1}; i_p^c{}_{red1}/v^{1/2}; \Delta E_{p\ red1}]$ shows the first reduction to be a quasi-reversible, diffusion-controlled one-electron process coupled to a chemical reaction (EC process[13]). The second reduction peak (Figure 8) occurs at the same potential as that of the disubstituted derivative **3a** (Table IV) and is therefore assigned to the formation of this complex at the electrode during the CV scan. This is also the case for the monosubstituted compounds with dppm, **7**, and with dppe, **12**. The oxidation peaks detected in addition to that of $\mathbf{2a}^{\bullet-}$ on the reverse scan of the CV are easily assigned to the oxidation of $1^{\bullet-}$ and of $(I^{\bullet-})$, generated at $E_{p\ red1}$ (Figure 8). The formation of $1^{\bullet-}$ and **3a** from the reduction of **2a** in the absence of added CO and $P(OMe)_3$ requires that both of these ligands be released from $\mathbf{2a}^{\bullet-}$. Thus, the reactions we have first considered are as follows:

$$\mathbf{2a}^{\bullet-} \rightleftharpoons (I^{\bullet-}) + P(OMe)_3 \qquad (4)$$

$$\mathbf{2a}^{\bullet-} \rightleftharpoons (II^{\bullet-}) + CO \qquad (5)$$

The combination of the free ligands with the coordinatively unsaturated metal species formed in reactions 4 and 5 would then lead to the detected products (reactions 1 and 6).

(15) If reaction 2 is reversible, the rate for the decay of $1^{\bullet-}$ becomes

$$-\frac{d[1^{\bullet-}]}{dt} = \frac{k_1 k_2 [1^{\bullet-}][P(OMe)_3] - k_{-1}k_{-2}[\mathbf{2a}^{\bullet-}][CO]}{k_{-1}[CO] + k_2[P(OMe)_3]}$$

where k_{-2} is the rate constant for the decomposition of $\mathbf{2a}^{\bullet-}$. From this expression it is still apparent that increasing [CO] will result in a decrease in the rate of decay of $1^{\bullet-}$.

(16) Zizelman, P. M.; Amatore, C.; Kochi, J. K. *J. Am. Chem. Soc.* **1984**, *106*, 3771.

$$(I^{\bullet-}) + CO \rightleftharpoons 1^{\bullet-} \quad (1)$$

$$(II^{\bullet-}) + P(OMe)_3 \rightleftharpoons \mathbf{3a}^{\bullet-} \xrightarrow[ETC]{\text{room temp}} \mathbf{3a} \quad (6)$$

However, in this reaction sequence, ($I^{\bullet-}$) would be an intermediate on the route to $1^{\bullet-}$, and this is not consistent with the low-temperature CV in Figure 9: this demonstrates that ($I^{\bullet-}$) cannot be an intermediate of the pathway to $1^{\bullet-}$ since the oxidation peak of the former is no longer detected whereas that of the latter is still present. We therefore conclude that ($I^{\bullet-}$) arises exclusively from $1^{\bullet-}$, via CO loss as shown above (Scheme IV). A mechanism consistent with these results will be discussed below (see Discussion).

Electrosynthesis of Disubstituted Derivatives of 1. Electrochemical Behavior of 2a in the Presence of $P(OMe)_3$. The effect that the addition of $P(OMe)_3$ produces on the CV of **2a** is similar to that described for **1** (see above). The substantial suppression of the primary reduction, the absence of the redox process of $1^{\bullet-}$ and ($I^{\bullet-}$), the enhancement of the second cathodic peak coincident with the reduction of **3a** are diagnostic of the occurrence of an ETC-catalyzed substitution process.

The kinetic analysis of the first reduction peak current of complex **2a** in the presence of various concentrations of ligand and at different scan rates shows that the experimental points deviate markedly from the theoretical curve predicted for an associative mechanism.[16] Therefore, the overall substitution in **2a** seems to be dominated by a dissociative process.

The electrosynthesis of **3a** is effected by reducing the singly substituted complex **2a** at its first cathodic peak in the presence of 1 equiv of $P(OMe)_3$. Complex **3a** can also be prepared from **1** and 2 equiv of $P(OMe)_3$ either in a direct manner by setting the electrolysis potential at −1.6 V or in a stepwise fashion (first electrolysis at −1.2 V followed by cpe at −1.6 V) (Table III).

Electrosynthesis of a Mixed $PMe_3/P(OMe)_3$ Disubstituted Complex. The same procedure as described above was used to electrosynthezise a disubstituted complex containing two different phosphorus ligands, e.g. $P(OMe)_3$ and PMe_3. The reduction of **2a** in the presence of 1 equiv of PMe_3 leads to the isolation of three different disubstituted compounds **3a**, **3c** (L/L = PMe_3/PMe_3), and **4** (Scheme V). The major product is the expected mixed $PMe_3/P(OMe)_3$ disubstituted derivative, isolated as a mixture of two isomers **4a** and **4b**. Spectral similarities [NMR (Table I) and IR and mass (Experimental Section)] for complexes **3c**–**4a,b** and **3a** suggest strongly that the phosphorus ligands occupy the P(5) and P(9) positions in all these derivatives. We have noticed that for all the monosubstituted derivatives studied here (**2a**$_1$ and **2a**$_2$; **7a** and **7b**; **12a** and **12b**) the resonance of the P atom at Fe(2) is more deshielded than that at Fe(1). On the basis of this observation we ascribe the structure drawn in Scheme V to the isomers **4a** and **4b**.

Electrosynthesis of Disubstituted Derivatives with Bidentate Ligands (dppm, dppe). The singly substituted derivatives **7** (dppm) and **12** (dppe) are characterized by a pseudoreversible reduction (Table IV) showing large anodic-to-cathodic peak separation and low anodic to cathodic peak current ratio. Reversible processes due to the disubstituted compounds generated at the electrode during the CV scan are detected at more negative potentials

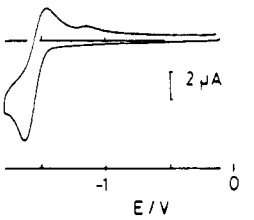

Figure 9. Cyclic voltammogram of a 0.7 mM solution of **2** at −10 °C in THF–[Bu_4N][PF_6] at a scan rate of 0.05 V·s^{-1} (vitreous carbon electrode).

(ca. −1.9 V, Table IV). An additional peak due to the acylated complex **10** ($E^{1/2}$ = −1.57 V) is observed in the CV of **7**.

The controlled-potential reduction of the monosubstituted complexes **7** and **12** at ca. −1.6 V in the absence of free dppm or dppe, respectively, leads to the Fe_2P_2 ring closure (Table III), and the disubstituted derivatives **8**, **13** (68% yield), and **14** (10% yield) are obtained. The product distribution with dppe contrasts with that resulting from thermal syntheses.

Electrochemistry of the Disubstituted Complex 3a. In the Absence of Ligands. The reduction of **3a** appears as a poorly reversible process (E_p = −2.0 V) in THF–[Bu_4N][PF_6] (inert atmosphere, room temperature). The current function $i_{p\,red}/v^{1/2} = f(v)$ shows a nonlinear behavior for scan rates below 0.2 V·s^{-1}, and this suggests the occurrence of an ECE type mechanism at $E_{p\,red1}$.[13] Other reduction processes at more negative potentials ($E_{p\,red}$ = −2.7 and −2.95 V) are assigned to products arising from the decomposition of $\mathbf{3a}^{\bullet-}$ and were not investigated further.

The stability of $\mathbf{3a}^{\bullet-}$ is increased at lower temperature (T = −10 °C), and under these conditions a second reduction, obscured at room temperature, is clearly apparent ($E_{p\,red2}$ = −2.20 V).

In the Presence of $P(OMe)_3$. The presence of free $P(OMe)_3$ stabilizes $\mathbf{3a}^{\bullet-}$: the chemical reversibility of the primary reduction, as measured by the ratio (i_p^a/i_p^c) increases from about 0.6 (no $P(OMe)_3$) to 0.75 (1 equiv of $P(OMe)_3$) and 0.90 (20 equiv of $P(OMe)_3$), whereas the primary reduction peak is slightly suppressed. This demonstrates that one chemical step coupled to the reduction of **3a** at $E_{p\,red1}$ consists of the reversible loss of a $P(OMe)_3$ ligand and generates the unsaturated intermediates $II^{\bullet-}$, Scheme VII. The presence of $P(OMe)_3$ also results in an increase of the second reduction (E_p = −2.29 V, 10 equiv of $P(OMe)_3$), also favored on decreasing the temperature. This step, which is assigned to the reduction of $\mathbf{3a}^{\bullet-}$, occurs at almost the same potential as the reduction of a tris-substituted $P(OMe)_3$ complex. Controlled-potential electrolyses of **3** performed at ca −2.0 V in the presence of an excess of free $P(OMe)_3$ lead to the tris-substituted complex, isolated in 67% yield as a mixture of two isomers **5a** and **5b**, with a reduction at E_p = −2.35 V.

Discussion

It was observed that the first carbonyl substitution reactions (thermal) by phosphites involve axial carbonyl ligands, e.g. C(5)O and C(9)O, to give a mixture of two isomers **2a**$_1$ and **2a**$_2$. By contrast, introduction of PPh_3 and dppm or dppe as monodentate ligands by CO substitution in cluster **1** involves equatorial carbonyl

Scheme V

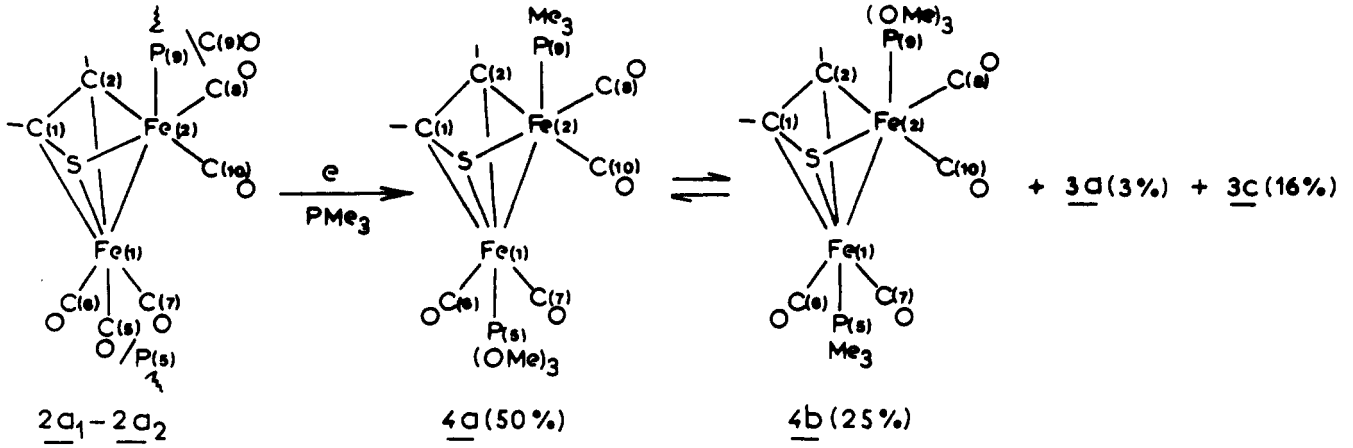

Scheme VI. Electron-Transfer-Chain-Catalyzed Substitution of a Phosphorus Ligand for CO in Complex 1[a]

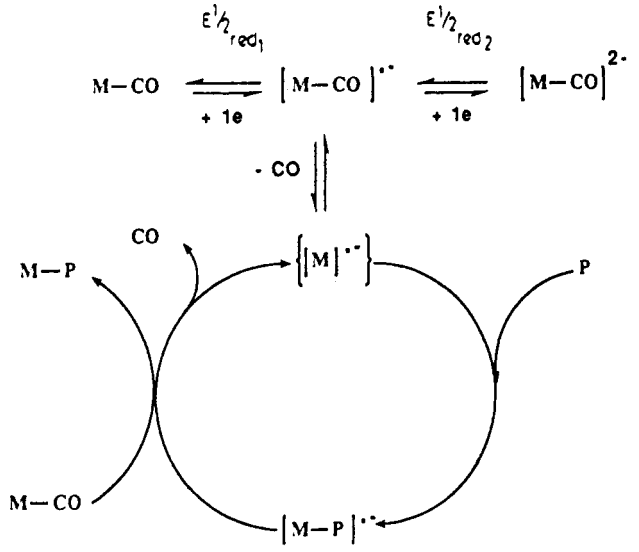

[a] M-CO stands for complex 1; M-P represents a singly substituted derivative, e.g. 2, 7, and 12.

ligands, e.g. C(6)O and C(10)O. The observation that equatorial isomers (**2b**, **7**, **12**) instead of axial isomers are formed with bulky diphosphines (PPh_3, dppm, dppe)[8] suggests that steric factors are important in determining the ligand coordination site. However, the formation of stable axial isomers $\mathbf{2a_1}$ and $\mathbf{2a_2}$ indicates that the two pairs of sites on the Fe–Fe unit, e.g. C(5)O–C(9)O and C(6)O–C(10)O, seem to have inequivalent acceptor requirements. Examination of the relative population ratios for $\mathbf{2_1}$:$\mathbf{2_2}$ ($\mathbf{2a_1}$:$\mathbf{2a_2}$ = 60:40; $\mathbf{2b_1}$:$\mathbf{2b_2}$ = 80:20) of the two isomers in $[Fe_2(CO)_5L\{\mu\text{-}(CF_3)C_2(CF_3)S\}]$ (**2**) (L = phosphite or phosphine), by integration of the respective signals in the ^{19}F NMR spectra, reveals that the major monosubstituted isomer fits with the Fe(1)-substituted species. However, with diphosphines (dppm, dppe) both the iron sites are nearly equivalent (**7a**:**7b** = **12a**:**12b** = 53:47).

These thermal reactions are not stereoselective, and they give mixtures of mono- and disubstituted derivatives with cluster **1**: L or L-L (L = PR_3; L-L = dppm, dppe), molar ratios greater than that of **1**. In each disubstituted complex, at least one phosphorus ligand occupies a site which is also P-substituted in the parent monosubstituted species. This observation is in good agreement with the quantitative conversion of the mixture of isomers **7a** (P(6)) and **7b** (P(10)) into **14a** (P(5)–P(6)) and **14b** (P(9)–P(10)) by heating in toluene. Formation of clusters containing four phosphite ligands, such as **6**, proceeds first by substitution of three Fe-bonded CO ligands (**5**) and needs light activation. However, the disubstituted derivatives involving tertiary phosphines and diphosphines acting as bridging ligands are obtained as single structural isomers (**3**, **8**, **13**, **10**, **15**), the monosubstituted complexes (**2**, **7**, **12**), the disubstituted derivatives involving dppm and dppe acting as chelating ligands (**9**, **14**), and the tris-substituted compounds (**5**) are formed as an equilibrium mixture of isomers which is independent of the temperature, as predicted thermodynamically, but which is slightly solvent dependent. In a dynamic NMR study, we shall discuss further (to be submitted for publication) the mechanism of the isomerization, $\mathbf{2_1} \rightleftharpoons \mathbf{2_2}$ and $m\mathbf{a} \rightleftharpoons m\mathbf{b}$ (m = 5, 7, 12, 9, 14).

The presence of two electron-withdrawing CF_3 groups in the (R)—C≡C—(R)—S ligand versus one or two Ph groups modifies the reactivity of clusters "Fe_2C_2S" (**1**). For example, disubstituted derivatives are mainly formed on reacting (thermal activation) two-electron donor ligands L (L = $P(OMe)_3$, PPh_3) with the cluster $[Fe(CO)_3\{\overline{Fe(CO)_3\text{---}CH\text{---}CPh\text{---}S}\}]$,[17] which is closely related to **1**. This contrasts sharply with our results which show that monosubstituted derivatives are obtained as major products (87–98% yields) in the reactions of the cluster **1** with tertiary phosphines. Moreover, by light activation in $[Fe(CO)_3\{\overline{Fe(CO)_3\text{---}CH\text{---}CPh\text{---}S}\}]$, only one or two carbonyl groups are replaced by phosphorus ligands,[17] whereas the third and the fourth carbonyl substitutions are reached in **1**. Our results show that the site of the first substitution reaction, which differs from that observed by Hickey et al.[7] and Huttner et al.,[17] depends sharply on the substituent located on the alkyne ligand. For example, that reaction involves the C(6)[17] and C(5)[7] positions, respectively, when $P(OMe)_3$ and PPh_3 are used as reactants with $[Fe(CO)_3\{\overline{Fe(CO)_3\text{---}CR\text{---}CPh\text{---}S}\}]$ (R = H,[17] Ph[7]), whereas the C(5) and C(6) positions, respectively, are here implied in $[Fe_2(CO)_6\{\mu\text{-}(CF_3)C_2(CF_3)S\}]$.

Electrochemical activation provides an alternative route to the substituted clusters. As shown by the results listed in Table III, the electrochemically initiated substitution (Scheme VI) is very efficient: the products are obtained

(17) Fässler, Th.; Huttner, G. *J. Organomet. Chem.* **1990**, *381*, 391.

Scheme VII. Reduction Mechanism of Complex 2a at Room Temperature under N_2 in a THF Electrolyte Showing a Dissociative Process (D) and a Fe–C (alkyne) σ Bond Cleavage Path (BC)[a]

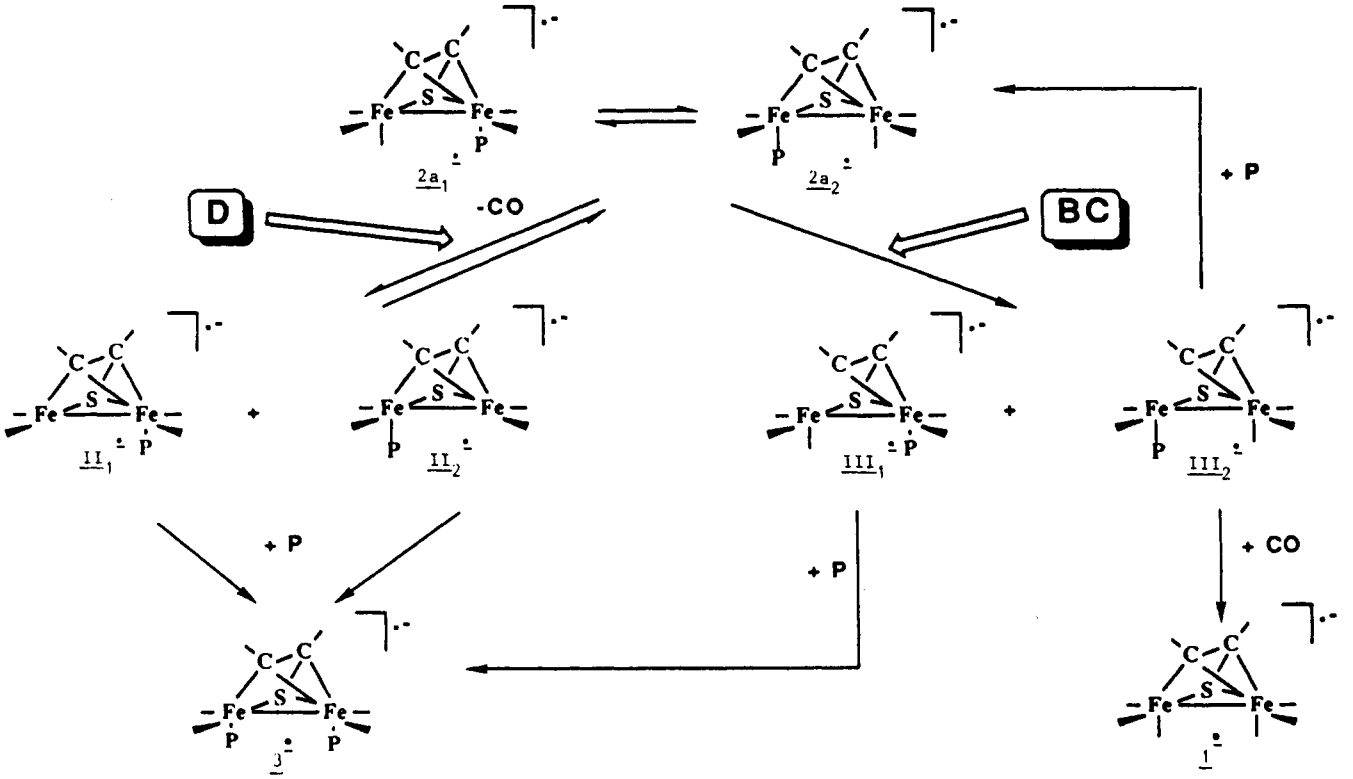

[a] P stands for $P(OMe)_3$; the CO ligands and CF_3 groups are omitted for clarity; the substituted coordination position shown may not correspond to the actual one.

selectively in high yields, with a low amount of electricity consumed and after short reaction times. We have shown above that the first substitution process in these reactions is dissociative. This result is similar to those recently reported by Hinkelman et al.[18] for the substitution of the $[Co_3(CO)_9(\mu_3\text{-CMe})]$ complex but is in sharp contrast with the associative nature of the substitution mechanism reported for $[Fe(CO)_3\{\overline{Fe(CO)_3\text{---}CH\text{---}CPh\text{---}S}\}]$,[19] a species closely related to 1. The isolation of singly substituted derivatives for the bidentate dppm and dppe ligands contrasts also with what we observed for $[Cp_2Co_4(CO)_4(\mu\text{-CO})(CF_3C_2CF_3)]$. Indeed, singly substituted derivatives of the tetracobalt cluster with dppm and dppe were observed only as intermediates on the CV time scale, and coordination of the dangling phosphine occurred thermally during electrolyses.[2b]

In the mechanism of the electrosynthesis of disubstituted complexes depicted in Scheme VII, we have considered that the occurrence of two isomers of **2a** could result in the formation of isomers of $2^{\bullet-}$ and of the unsaturated intermediates involved. Two different pathways are shown for the decomposition of $2^{\bullet-}$. As in reaction 5, CO is released according to the dissociative path D which results in the first type of coordinatively unsaturated intermediates retaining the phosphorus ligand ($II_1^{\bullet-}$ and $II_2^{\bullet-}$). The second process leading to the exposure of a coordination site in $III_1^{\bullet-}$ and $III_2^{\bullet-}$ via the cleavage of the Fe–C (alkyne) σ bond (path BC in Scheme VII) could result from a partial rotation of the alkyne moiety, induced by electronation. The BC component of Scheme VII is similar to the associative mechanism recently proposed for the ETC-catalyzed substitution of $[Fe(CO)_3\{\overline{Fe(CO)_3\text{---}CH\text{---}CPh\text{---}S}\}]$.[19] The reactions in Scheme VII show that reaction of CO or $P(OMe)_3$ with the intermediates $II^{\bullet-}$ (1 and 2) and $III^{\bullet-}$ (1 and 2) leads to the detected products, $1^{\bullet-}$ and **3**, whereas the formation of $I^{\bullet-}$ as an intermediate is avoided. In addition, an intermediate such as $III_1^{\bullet-}$ where P is a dppm ligand might be at the origin of the disubstituted derivative **10**. The effect of CO on the reduction of **2** (Figure 10) lends further support to the reaction sequence in Scheme VII. The enhancement of the oxidation peak current for $1^{\bullet-}$ and the suppression of the second reduction can be rationalized by the fact

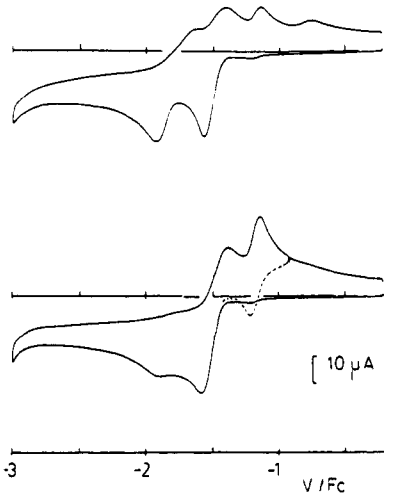

Figure 10. Cyclic voltammograms of a 0.9 mM solution of **2a** under N_2 (top) and under CO (bottom) in THF–$[Bu_4N][PF_6]$ (scan rate 0.2 $V \cdot s^{-1}$; vitreous carbon electrode).

(18) Hinkelmann, K.; Heinze, J.; Schacht, H. T.; Field, J. S.; Vahrenkamp, H. *J. Am. Chem. Soc.* **1989**, *111*, 5078.

(19) Fässler, Th.; Huttner, G.; Günauer, D.; Fiedler, S.; Eber, B. *J. Organomet. Chem.* **1990**, *381*, 409.

that CO prevents the formation of intermediates of type II. Therefore, $1^{\bullet-}$ produced along path BC would be favored at the expense of $3^{\bullet-}$. The enhancement of the primary reduction of **2** in the presence of CO is assigned to the reversible reduction of $1^{\bullet-}$ at nearly the same potential.

When the electrolysis of **2a** was performed in the presence of PMe_3, in addition to the mixed disubstituted derivative **4**, compounds **3a** and **3c** are formed; this is consistent with the reaction Scheme VII. Indeed, the reaction of free PMe_3 with $III_2^{\bullet-}$ would produce the PMe_3 singly substituted complex which, in turn, undergoes an ETC-catalyzed substitution of PMe_3 for CO to yield **3c**. The $P(OMe)_3$ ligand released in the above process can react with any of the intermediates $II_1^{\bullet-}$, $II_2^{\bullet-}$, or $III_1^{\bullet-}$ to produce **3a**, whereas the addition of PMe_3 to these intermediates affords the major product **4**. This result suggests that some of the homodisubstituted complex **3a** formed when **2a** is reduced in the presence of $P(OMe)_3$ might also arise from path BC (Scheme VII). Accordingly, path D appears as the major, but not exclusive, route to complex **3a**.

Concerning the formation of the acylated complexes, similar behaviors are observed in thermal and electrochemical reactions. The production of the acylated compound with dppm and not with dppe or $P(OMe)_3$ cannot be explained solely in terms of electronic factors since all the phosphorus ligands used in this study affect the redox potential of **1** in a very similar way (see Table IV). Thus, the different behavior of dppm, dppe, and $P(OMe)_3$ during the formation of an acylated species might partly lie in the existence of geometric constraints. Whether or not a dppe analogue of **10** or $10^{\bullet-}$ (e.g. **15** or $15^{\bullet-}$) is formed transiently in the electrosyntheses is unclear. Although it is less stable than **10**, **15** requires heating to convert to **12** or **14**. It is therefore unlikely that **15** would decay to these species during cpe which is performed at room temperature and is complete in a few minutes (Table III). The CV of **15** shows that it undergoes a reversible one-electron reduction $[(i_p^a/i_p^c)_{red1} = 1.0]$, with no sign of formation of either **12** or **14**. All these facts suggest that the acylated species **15** is not produced, even transiently, in the reductively initiated electrosyntheses.

Summary

We have shown that the thermal reactions of the diiron complex **1** with trimethyl phosphite, triphenylphosphine, and diphosphines (dppm, dppe) give mixtures of mono- and disubstituted products in a nonstereoselective way. These ligand substitution reactions are very sensitive to the properties and to the size of the nucleophile: the reaction with $P(OMe)_3$ gives a different type of product than is obtained with PPh_3 or diphosphines. Introduction of PPh_3, dppm, or dppe as monodentate ligands by CO substitution in **1** involves the equatorial CO ligands, whereas axial positions are substituted when trimethyl phosphite is used. UV irradiation gives tri- and tetrasubstituted complexes.

Furthermore, electrochemical activation provides an alternative route to the substituted clusters which are obtained selectively with a low amount of electricity consumed. We have shown that the first substitution process in these reactions is dissociative.

Experimental Section

The reactions were performed under a nitrogen atmosphere using standard Schlenk techniques, and solvents were deoxygenated and dried by standard methods. The irradiation of the products was made using a Philips HPK 125-W mercury vapor lamp immersed in the THF solution of the products and by bubbling nitrogen through the solution.

The electrochemical experiments were performed as described previously.[2b] They were carried out in a thermostated cell (Methrom) at room temperature. The potentials are quoted relative to the ferrocene–ferrocenium cation couple, ferrocene being added as an internal standard at the end of the CV experiments.

Infrared spectra were obtained with a Perkin-Elmer 1430 spectrophotometer in hexane or dichloromethane solutions in the ν(CO) region. The mass spectra were measured on a Varian MAT 311 in the "Mesures Physiques" laboratory, University of Rennes, or on a GC/MS Hewlett-Packard 5995C. NMR spectra (^{13}C, ^{19}F, ^{31}P), in $CDCl_3$ solution, were recorded on a JEOL FX 100 or a Bruker AC 300 and were referenced to Me_4Si, $CFCl_3$, and $H_3(PO_4)$, respectively. Chemical analyses were performed by the "Centre de Microanalyses du CNRS de Lyon".

The bimetallic complex $[(CO)_3Fe\{\mu\text{-}(CF_3C_2CF_3)S\}Fe(CO)_3]$ was prepared as described previously.[6] All other reagents were commercial grade and were used as obtained.

Thermal Reaction of $[(CO)_3Fe\{\mu\text{-}(CF_3C_2CF_3)S\}Fe(CO)_3]$ (I) with Mono- and Diphosphines. In a typical procedure ca. 0.2 g of **1** (0.42 mmol) was dissolved in THF (50 cm^3) and n equiv of phosphine, phosphite, or diphosphine [n = 0.5 (dppe); n = 1 ($P(OMe)_3$, PPh_3, dppm); n = 2 (dppm, dppe); n = 10 ($P(OMe)_3$)] was added under nitrogen. The reaction mixture was refluxed for 24 h. After evaporation of the solvent in vacuo, the residue was extracted with CH_2Cl_2 and the solution was chromatographed on silica gel column. The products were eluted with mixtures of hexane–dichloromethane or dichloromethane–ether. Removal of solvent in vacuo afforded red mono- or disubstituted derivatives.

$2a_1$ and $2a_2$: eluted with hexane–CH_2Cl_2 (90:10) [yield: 98% (n = 1); 20% (n = 10)]. Anal. Calcd for $C_{12}H_9F_6Fe_2O_8PS$: C, 25.3; H, 1.6; P, 5.5. Found: C, 26.0; H, 1.7; P, 5.7. IR: ν(CO) 2076 (s), 2027 (s), 2016 (s), 2004 (s), 1986 (w), 1974 (w) cm^{-1} (hexane). Mass spectrum: m/z 570 (M^+), other peaks, $M^+ - x$CO (x = 1–5), 336 ($M^+ - 5CO - FeF_2$).

$2b_1$ and $2b_2$: eluted with hexane–CH_2Cl_2 (90:10) [yield: 87% (n = 1)]. Anal. Calcd for $C_{27}H_{15}F_6Fe_2O_5PS$: C, 45.5; H, 2.6. Found: C, 44.8; H, 3.0. IR: ν(CO) 2084 (s), 2080 (s), 2063 (s) cm^{-1} (CH_2Cl_2).

3a: eluted with hexane–CH_2Cl_2 (80:20) [yield: 80% (n = 10)]. Anal. Calcd for $C_{14}H_{18}F_6Fe_2O_{10}P_2S$: C, 25.3; H, 2.7; P, 9.3. Found: C, 25.3; H, 2.7; P, 10.1. IR: ν(CO) 2036 (s), 1998 (s), 1972 (s), 1945 (w) cm^{-1} (hexane). Mass spectrum: m/z 666 (M^+), other peaks, $M^+ - x$CO (x = 1–4), 430 ($M^+ - 4$ CO $- P(OMe)_3$), 306 ($M^+ - 4CO - 2P(OMe)_3$), 212 ($M^+ - 4CO - 2P(OMe)_3 - FeF_2$).

3b: eluted with hexane–CH_2Cl_2 (80:20) [yield: 80% (n = 10)]. Anal. Calcd for $C_{44}H_{30}F_6Fe_2O_4P_2S$: C, 56.1; H, 3.2; P, 6.6. Found: C, 56.2; H, 3.2; P, 6.8. IR: ν(CO) 2020 (s), 1987 (s), 1956 (s), 1925 (w) cm^{-1} (hexane).

7a and 7b: eluted with hexane–CH_2Cl_2 (80:20) [yield: 61% (n = 1); 43% (n = 2)]. Anal. Calcd for $C_{34}H_{22}F_6Fe_2O_5P_2S$: C, 49.1; H, 2.6; P, 7.4. Found: C, 49.1; H, 2.6; P, 6.8. IR: ν(CO) 2070 (s), 2016 (sh), 2006 (s), 1960 (w) cm^{-1} (CH_2Cl_2). Mass spectrum: m/z 830 (M^+), other peaks, $M^+ - x$CO (x = 1–5).

8: eluted with hexane–CH_2Cl_2 (70:30) [yield: 3.5% (n = 1); 12% (n = 2)]. Anal. Calcd for $C_{33}H_{22}F_6Fe_2O_4P_2S$: C, 49.4; H, 2.7; Fe, 13.9; P, 7.6. Found: C, 49.7; H, 2.7; Fe, 13.3; P, 7.6. IR: ν(CO) 2021 (m), 1984 (s), 1964 (m), 1924 (w) cm^{-1} (CH_2Cl_2). Mass spectrum: m/z 802 (M^+), other peaks, $M^+ - x$CO (x = 1–4), 596 ($M^+ - 4CO - FeF_2$).

9a and 9b: eluted with hexane–CH_2Cl_2 (70:30) [yield: traces (n = 1); 2% (n = 2)].

10: eluted with CH_2Cl_2–ether (90:10) [yield: 35% (n = 2)]. Anal. Calcd for $C_{34}H_{22}F_6Fe_2O_5P_2S$: C, 49.2; H, 2.7; F, 13.8; Fe, 13.5; P, 7.5. Found: C, 49.9; H, 2.7; F, 13.9; Fe, 13.7; P, 7.6. IR: ν(CO) 2026 (m), 1995 (s), 1959 (m), 1945 (w), 1632 (m) cm^{-1} (CH_2Cl_2). Mass spectrum: m/z 830 (M^+), other peaks, $M^+ - xCO$ (x = 1–5), 596 ($M^+ - 5CO - FeF_2$).

11: eluted with hexane [yield: 86% (n = 0.5)]. The complex crystallized with two molecules of pentane and one of dichloromethane. Anal. Calcd for $C_{55}H_{50}Cl_2F_{12}Fe_4O_{10}P_2S_2$: C, 43.5; H, 3.3; Fe, 14.7; P, 4.0. Found: C, 43.8; H, 2.9; Fe, 14.6; P, 3.5. IR: ν(CO) 2070 (s), 2010 (s), 1964 (w) cm^{-1} (CH_2Cl_2). Mass spectrum: m/z 1290 (M^+), other peaks, $M^+ - xCO$ (x = 1–5).

12a and 12b: eluted with hexane–CH_2Cl_2 (80:20) [yield: 34% (n = 2)]. Anal. Calcd for $C_{35}H_{24}F_6Fe_2O_5P_2S$: C, 49.8; H, 2.8; Fe, 13.2. Found: C, 49.0; H, 3.1; Fe, 13.5. IR: ν(CO) 2072 (s), 2016 (sh), 2006 (s), 1960 (w) cm^{-1} (CH_2Cl_2). Mass spectrum: m/z 844 (M^+), other peaks, $M^+ - xCO$ (x = 1–5).

13: eluted with hexane–CH_2Cl_2 (70:30) [yield: <1% (n = 2)]. Anal. Calcd for $C_{34}H_{24}F_6Fe_2O_4P_2S$: C, 50.0; H, 2.9; P, 7.6. Found: C, 50.0; H, 2.9; P, 7.5. IR: ν(CO) 2018 (m), 1980 (s), 1958 (m), 1925 (w) cm^{-1} (CH_2Cl_2). Mass spectrum: m/z 816 (M^+), other peaks, $M^+ - xCO$ (x = 1–4), 610 ($M^+ - 4CO - FeF_2$).

14a and 14b: eluted with hexane–CH_2Cl_2 (70:30) [yield: 48% (n = 2)]. Anal. Calcd for $C_{34}H_{24}F_6Fe_2O_4P_2S$: C, 50.0; H, 2.9; Fe, 13.7; P, 7.6. Found: C, 50.4; H, 3.4; Fe, 13.0; P, 7.5. IR: ν(CO) 2042 (m), 1975 (m), 1945 (m) cm^{-1} (CH_2Cl_2).

15: eluted with CH_2Cl_2–ether (90:10) [yield: 4.5% (n = 2)]. Anal. Calcd for $C_{35}H_{24}F_6Fe_2O_5P_2S$: C, 49.8; Fe, 13.2. Found: C, 49.8; Fe, 13.6. IR: ν(CO) 2028 (m), 1996 (s), 1070 (m), 1944 (w), 1630 (m) cm^{-1} (CH_2Cl_2).

Photolytic Reaction of $[(CO)_3Fe\{\mu\text{-}(CF_3C_2CF_3)S\}Fe(CO)_3]$ (1) with Phosphite. A large excess of phosphite (4.2 mmol) was added to a THF solution of 1 (0.21 mmol). The mixture was stirred at room temperature and irradiated for 15 min. The solution was then evaporated to dryness, the residue was redissolved in a minimum of CH_2Cl_2, and the solution was chromatographed on silica gel. Elution with hexane–CH_2Cl_2 (90:10) afforded a red band, from which complex **2** was isolated (8%). Elution with hexane–CH_2Cl_2 (80:20) served to remove the red band, which was evaporated to yield product **3a** (20%). Further elution with hexane–CH_2Cl_2 (40:60) gave a red fraction, from which **5** (40%) was obtained. Finally, elution with CH_2Cl_2 afforded a dark-red fraction of **6** (12%).

When the irradiation time was prolonged to 90 min, **3**, **5**, and **6** were isolated in 3.5, 11, and 56% yields, respectively.

5a and 5b. IR: ν(CO) 1995 (s), 1943 (s) cm^{-1} (CH_2Cl_2). Mass spectrum: m/z 762 (M^+), other peaks, $M^+ - xCO$ (x = 1–3), 554 ($M^+ - 3CO - P(OMe)_3$), 430 ($M^+ - 3CO - 2P(OMe)_3$), 306 ($M^+ - 3CO - 3P(OMe)_3$), 212 ($M^+ - 3CO - 3P(OMe)_3 - FeF_2$).

6. Anal. Calcd for $C_{18}H_{36}F_6Fe_2O_{14}P_4S$: C, 25.2; H, 4.2. Found: C, 25.7; H, 4.3. IR: ν(CO) 1934 (m), 1895 (w) cm^{-1} (CH_2Cl_2). Mass spectrum: m/z 858 (M^+), other peaks, 706 ($M^+ - CO - P(OMe)_3$), 554 ($M^+ - 2CO - 2P(OMe)_3$), 460 ($M^+ - 2CO - 2P(OMe)_3 - FeF_2$), 336 ($M^+ - 2CO - 3P(OMe)_3 - FeF_2$).

Electrochemical Synthesis of the Mixed Complex $[(CO)_2\{P(OMe)_3\}Fe\{\mu\text{-}(CF_3C_2CF_3)S\}Fe(PMe_3)(CO)_2]$ (4). Complex **2a** (0.1 g) was dissolved in 30 mL of a THF electrolyte and electrolyzed under N_2 at its first cathodic peak in the presence of 1 equiv of PMe_3. The catholyte was syringed out of the cell and transferred to a Schlenk flask. The THF was removed and the residue was chromatographed on silica gel. Elution with hexane–CH_2Cl_2 (80:20) served to remove two red bands, which were evaporated to yield products **3a** (3%) and **3c** (16%), respectively. Further elution with hexane–CH_2Cl_2 (20:80) yielded a red fraction of **4** (75%).

3c: eluted with hexane–CH_2Cl_2 (80:20). IR: ν(CO) 2015 (s), 1972 (s), 1940 (s), 1917 (m) cm^{-1} (hexane). Mass spectrum: m/z 570 (M^+), other peaks, $M^+ - xCO$ (x = 1–4).

4a and 4b. IR: ν(CO) 2024 (s), 1984 (s), 1955 (s), 1932 (w) cm^{-1} (hexane). Mass spectrum: m/z 618 (M^+), other peaks, $M^+ - xCO$ (x = 1–4).

Table V. Crystallographic Data and Refinement Details for the Complexes $[Fe_2(CO)_{6-n}\{P(OMe)_3\}_n\{\mu\text{-}(CF_3)C_2(CF_3)S\}]$, Where n = 1–3

	n = 1	n = 2	n = 3
formula	$C_{12}H_9F_6Fe_2O_8PS$	$C_{14}H_{18}F_6Fe_2O_{10}P_2S$	$C_{16}H_{27}F_6Fe_2O_{12}P_3S$
fw	569.92	665.98	762.05
cryst syst	monoclinic	orthorhombic	triclinic
space group	$P2_1/n$	$P2_12_12_1$	$P\bar{1}$
a (Å)	7.584 (1)	10.646 (6)	9.447 (5)
b (Å)	24.563 (4)	13.051 (4)	10.740 (1)
c (Å)	11.028 (2)	18.258 (7)	16.205 (4)
α (deg)			108.20 (1)
β (deg)	97.41 (2)		92.51 (3)
γ (deg)			110.22 (2)
U (Å^3)	2037.2 (6)	2537 (2)	1444.3 (10)
Z	4	4	2
D_{calcd} (g cm^{-3})	1.858	1.744	1.752
F(000)	1128	1336	772
μ (cm^{-1})	16.9	14.3	13.3
cryst size (mm)	0.23 × 0.08 × 0.16	0.25 × 0.10 × 0.10	0.33 × 0.30 × 0.27
θ range (deg)	2–23	2–22	2–23
h	0–8	0–11	$\bar{10}$–10
k	$\bar{27}$–27	$\bar{13}$–4	$\bar{11}$–11
l	$\bar{12}$–12	$\bar{19}$–19	$\bar{17}$–17
no. of reflns measd	6045	4858	8004
no. of unique reflns	2827	1788	4002
no. of obsd reflns	1709	1129	2577
R_{int}	0.028	0.062	0.026
R	0.027	0.064	0.036
R_w	0.028	0.052	0.038
no. of params	271	290	358
$\|\Delta\rho\|$ (e/Å^3)	0.35	0.46	0.43
S	1.6	3.0	1.9

Crystal Structures of $[Fe_2(CO)_{6-n}\{P(OMe)_3\}_n\{\mu\text{-}(CF_3)C_2(CF_3)S\}]$, n = 1–3. Similar experimental and computational methods were used for all three structures (Table II). Measurements were made at 22 °C with Mo Kα X-rays, λ = 0.710 69 Å, on an Enraf-Nonius CAD4 diffractometer fitted with a graphite monochromator. Cell dimensions were obtained from least-squares treatments of the setting angles of ≥20 high-angle reflections. Intensities were determined from $\omega/2\theta$ scans of 0.70–0.80° in ω and were corrected for Lp and absorption[20] effects. The structures were solved by Patterson and Fourier methods. They were then refined on F with $w = 1/\sigma(F)^2$ to convergence ($\Delta/\sigma \leq 0.20$) by the method of full-matrix least-squares using reflections with $I \geq k\sigma(I)$ (k = 3 for n = 1; k = 2 for n = 2 and 3). With the exceptions noted below for the n = 2 and n = 3 complexes, anisotropic displacement parameters were refined for non-H atoms and allowance was made for the scattering of the H atoms. H atoms were initially positioned to give staggered conformations across O–C bonds and were then constrained to ride on their parent C atoms with C–H = 0.96 Å and U(H) = 1.2U(C). Neutral atom scattering factors and anomalous dispersion corrections were taken from ref 21 and the calculations were performed on a VAX3600 with the GX package.[22] Final parameters for non-hydrogen atoms are presented in Table VI.

For the n = 2 complex a crystal of suitable quality was difficult to obtain and the accuracy of the analysis is low because of the small number of observed intensities and their poor internal consistency (R_{int} = 0.062). For the final calculations Friedel pairs were merged and anomalous dispersion corrections were not applied. C(22) and C(23) are each disordered over two sites, the more heavily populated of which has respective occupancies of 0.75 (3) and 0.58 (3); for these disordered C atoms a single isotropic U parameter was refined. Individual isotropic U parameters were refined for other methyl carbon atoms, and no H atoms were included in the calculations.

(20) Walker, N.; Stuart, D. *Acta Crystallogr.* **1983**, *A39*, 158.
(21) *International Tables for X-ray Crystallography*; Kynoch: Birmingham, 1974; Vol. 4, pp 99, 119.
(22) Mallinson, P. R.; Muir, K. W. *J. Appl. Crystallogr.* **1985**, *18*, 51.

Table VI. Fractional Coordinates and Equivalent Isotropic Displacement Parameters (Å²)[a]

	x	y	z	U		x	y	z	U
			(a) $[Fe_2(CO)_5\{P(OMe)_3\}\{\mu\text{-}(CF_3)C_2(CF_3)S\}]$ (**2a**$_1$)						
Fe(1)	0.21561 (9)	0.13244 (2)	0.27614 (5)	0.038	O(11)	0.0723 (5)	0.0974 (2)	0.5318 (3)	0.068
Fe(2)	0.01205 (10)	0.16462 (3)	0.09091 (6)	0.047	O(12)	0.3788 (5)	0.1382 (1)	0.5436 (3)	0.075
S	−0.04983 (16)	0.09390 (5)	0.21112 (10)	0.044	O(13)	0.3087 (5)	0.0417 (1)	0.4787 (3)	0.073
P(1)	0.24076 (17)	0.10150 (5)	0.46191 (10)	0.044	C(1)	0.1441 (6)	0.0680 (2)	0.1639 (4)	0.043
F(1)	0.1697 (6)	−0.0158 (1)	0.0666 (3)	0.106	C(2)	0.2004 (6)	0.1110 (2)	0.0949 (4)	0.048
F(2)	0.3624 (5)	0.0003 (1)	0.2185 (3)	0.100	C(3)	0.1936 (9)	0.0085 (2)	0.1754 (5)	0.068
F(3)	0.0978 (6)	−0.0174 (1)	0.2481 (3)	0.105	C(4)	0.3475 (10)	0.1059 (3)	0.0166 (5)	0.085
F(4)	0.4808 (6)	0.0739 (2)	0.0631 (4)	0.127	C(6)	0.4485 (8)	0.1379 (2)	0.2911 (4)	0.058
F(5)	0.2856 (6)	0.0832 (2)	−0.0899 (3)	0.143	C(7)	0.1808 (7)	0.2006 (2)	0.3175 (4)	0.059
F(6)	0.4195 (6)	0.1524 (2)	−0.0070 (4)	0.125	C(8)	0.1284 (9)	0.2195 (2)	0.0344 (5)	0.080
O(2)	0.6003 (6)	0.1413 (2)	0.3028 (4)	0.095	C(9)	−0.1046 (9)	0.1455 (2)	−0.0527 (5)	0.068
O(3)	0.1683 (7)	0.2448 (2)	0.3492 (3)	0.099	C(10)	−0.1562 (8)	0.2101 (2)	0.1378 (5)	0.065
O(4)	0.2007 (8)	0.2556 (2)	−0.0020 (5)	0.139	C(11)	−0.0414 (9)	0.1431 (3)	0.5434 (5)	0.084
O(5)	−0.1754 (7)	0.1338 (2)	−0.1460 (4)	0.104	C(12)	0.4390 (10)	0.1294 (3)	0.6710 (5)	0.103
O(6)	−0.2584 (7)	0.2394 (2)	0.1653 (4)	0.103	C(13)	0.2689 (9)	0.0016 (2)	0.5653 (5)	0.084
			(b) $[Fe_2(CO)_4\{P(OMe)_3\}_2\{\mu\text{-}(CF_3)C_2(CF_3)S\}]$ (**3a**$_1$)[b]						
Fe(1)	0.00888 (26)	−0.02090 (22)	0.09240 (15)	0.045	O(22)	0.4216 (15)	−0.1217 (14)	0.2345 (11)	0.102
Fe(2)	0.22296 (23)	0.01157 (29)	0.14859 (15)	0.051	O(23)	0.4372 (15)	0.0686 (12)	0.2595 (11)	0.111
S	0.0366 (5)	0.0570 (4)	0.2022 (3)	0.051	C(1)	0.0112 (20)	−0.0766 (17)	0.1929 (12)	0.056
P(1)	−0.1859 (5)	0.0196 (6)	0.0739 (3)	0.050	C(2)	0.1183 (18)	−0.1103 (20)	0.1590 (12)	0.048
P(2)	0.3394 (5)	−0.0169 (6)	0.2431 (3)	0.067	C(3)	−0.0780 (24)	−0.1343 (24)	0.2421 (14)	0.063
F(1)	−0.0331 (12)	−0.1553 (11)	0.3096 (7)	0.094	C(4)	0.1516 (25)	−0.2139 (24)	0.1511 (15)	0.071
F(2)	−0.1253 (15)	−0.2142 (12)	0.2176 (9)	0.110	C(6)	0.0040 (27)	−0.1125 (19)	0.0265 (12)	0.071
F(3)	−0.1773 (11)	−0.0669 (12)	0.2574 (7)	0.096	C(7)	0.0683 (24)	0.0676 (21)	0.0339 (13)	0.071
F(4)	0.0600 (15)	−0.2768 (10)	0.1265 (7)	0.098	C(8)	0.3245 (22)	−0.0380 (21)	0.0864 (12)	0.070
F(5)	0.1842 (14)	−0.2616 (9)	0.2162 (9)	0.095	C(10)	0.2764 (24)	0.1321 (24)	0.1291 (15)	0.089
F(6)	0.2402 (14)	−0.2371 (10)	0.1037 (9)	0.098	C(11)	−0.1853 (27)	0.2177 (24)	0.1002 (14)	0.107 (10)
O(2)	0.0009 (20)	−0.1750 (13)	−0.0195 (9)	0.105	C(12)	−0.3316 (23)	0.0531 (19)	−0.0408 (12)	0.090 (8)
O(3)	0.1033 (16)	0.1273 (15)	−0.0131 (9)	0.099	C(13)	−0.3038 (27)	−0.1620 (24)	0.0743 (15)	0.106 (10)
O(4)	0.3915 (16)	−0.0663 (16)	0.0413 (9)	0.107	C(21)	0.2165 (25)	0.0483 (18)	0.3645 (13)	0.092 (8)
O(6)	0.3062 (18)	0.2220 (16)	0.1194 (10)	0.106	C(22A)[c]	0.531 (11)	−0.169 (8)	0.208 (6)	0.093 (8)
O(11)	−0.2420 (12)	0.1199 (14)	0.1097 (10)	0.090	C(22B)[a]	0.491 (3)	−0.172 (2)	0.292 (2)	0.093
O(12)	−0.2069 (12)	0.0287 (12)	−0.0104 (6)	0.071	C(23A)[a]	0.554 (7)	0.083 (6)	0.254 (4)	0.093
O(13)	−0.2968 (13)	−0.0566 (15)	0.1028 (8)	0.085	C(23B)[c]	0.530 (4)	0.070 (3)	0.318 (2)	0.093
O(21)	0.2747 (14)	−0.0344 (12)	0.3206 (8)	0.094					
			(c) $[Fe_2(CO)_3\{P(OMe)_3\}_3\{\mu\text{-}(CF_3)C_2(CF_3)S\}]$ (**5a**)						
Fe(1)	0.16173 (7)	−0.28092 (7)	0.19784 (4)	0.036	O(23)[d]	0.4174 (7)	0.3251 (7)	0.3183 (4)	0.061 (2)
Fe(2)	0.27258 (8)	−0.00902 (7)	0.24999 (4)	0.038	O(23′)[d]	0.4457 (13)	0.3187 (12)	0.3930 (8)	0.061
S	0.36515 (14)	−0.13935 (13)	0.30702 (9)	0.045	O(31)	0.5329 (4)	−0.0480 (4)	0.1409 (3)	0.059
P(1)	0.21749 (14)	−0.46803 (13)	0.16702 (9)	0.043	O(32)	0.4640 (5)	0.1542 (4)	0.1319 (3)	0.069
P(2)	0.31064 (18)	0.18451 (16)	0.35278 (11)	0.063	O(33)	0.6357 (4)	0.1896 (4)	0.2596 (2)	0.055
P(3)	0.48003 (15)	0.07303 (13)	0.19609 (9)	0.043	C(1)	0.1772 (6)	−0.2004 (5)	0.3293 (3)	0.045
F(1)	0.1524 (6)	−0.1760 (4)	0.4753 (2)	0.118	C(22)	0.1082 (6)	−0.1277 (5)	0.2921 (3)	0.041
F(2)	0.0030 (4)	−0.3686 (4)	0.3791 (2)	0.094	C(3)	0.1414 (8)	−0.2693 (6)	0.3965 (4)	0.065
F(3)	0.2369 (5)	−0.3306 (4)	0.4069 (3)	0.116	C(4)	−0.0487 (7)	−0.1319 (6)	0.3041 (4)	0.062
F(4)	−0.1526 (3)	−0.2594 (3)	0.2990 (2)	0.084	C(6)	−0.0315 (7)	−0.3866 (6)	0.1519 (3)	0.046
F(5)	−0.0493 (4)	−0.0436 (4)	0.3825 (2)	0.096	C(7)	0.2016 (6)	−0.2458 (5)	0.0998 (4)	0.043
F(6)	−0.1125 (4)	−0.0967 (4)	0.2450 (3)	0.103	C(8)	0.1618 (7)	0.0279 (6)	0.1792 (4)	0.050
O(2)	−0.1575 (5)	−0.4560 (4)	0.1226 (3)	0.063	C(11)	0.5023 (7)	−0.3677 (7)	0.1451 (6)	0.093
O(3)	0.2143 (5)	−0.2380 (4)	0.0314 (3)	0.061	C(12)	0.1743 (8)	−0.6970 (6)	0.0288 (4)	0.075
O(4)	0.0879 (5)	0.0483 (4)	0.1306 (3)	0.077	C(13)	0.0040 (8)	−0.6507 (7)	0.2143 (5)	0.074
O(11)	0.3912 (4)	−0.4530 (4)	0.1817 (3)	0.064	C(21)	0.3789 (11)	0.1579 (9)	0.5070 (6)	0.108
O(12)	0.1522 (4)	−0.5654 (4)	0.0667 (2)	0.055	C(22)	0.1536 (8)	0.3371 (8)	0.4300 (5)	0.089
O(13)	0.1638 (4)	−0.5740 (4)	0.2197 (3)	0.056	C(23)	0.4947 (11)	0.4503 (9)	0.3627 (6)	0.112
O(21)[d]	0.4125 (7)	0.2404 (7)	0.4428 (4)	0.061 (2)	C(31)	0.6677 (7)	−0.0210 (7)	0.0995 (5)	0.075
O(21′)[d]	0.2893 (15)	0.1448 (13)	0.4623 (8)	0.061	C(32)	0.5609 (8)	0.2820 (7)	0.1276 (5)	0.089
O(22)	0.1611 (4)	0.2173 (4)	0.3631 (3)	0.062	C(33)	0.7016 (7)	0.1665 (8)	0.3329 (5)	0.084

[a] Apart from the exceptions indicated in parts b and c U is defined by $U = {}^1/_3\sum_{i=1}^{3}\sum_{j=1}^{3}U_{ij}a_i^*a_j^*(\vec{a}_i\cdot\vec{a}_j)$. [b] For methyl carbon atoms C(11)–C(23B) U is the isotropic displacement parameter. [c] Note: A common U was refined for C(22A)–C(23B). C(22A) and C(22B) have occupancies p and $1-p$ with $p = 0.25$ (3); similarly, $p = 0.42$ (3) for C(23A)/C(23B). [d] Note: Disordered oxygen atoms O(21) and O(23) were assigned a common occupancy, p, and O(21′) and O(23′) occupancy $1-p$ where $p = 0.641$ (4) at the end of the refinement. For these atoms isotropic displacement parameters were refined with U[O(21′)] = U[O(21)] and U[O(23′)] = U[O(23)]. Distances and angles involving these atoms are subject to large systematic errors because of disorder.

The P(2) phosphite is also disordered in the $n = 3$ complex: O(21) and O(23) are each distributed over two sites with occupancies 0.641 (3) and 0.359 (3); a single isotropic U parameter was refined for the four disordered O sites, and the H atoms attached to C(21) and C(23) were not included in the calculations.

Acknowledgment. CNRS, Brest University (F.R., R.R., J.T. and F.Y.P.), and Glasgow University are acknowledged for financial support. We are grateful to Dr. R. Pichon (Brest) for assistance in NMR experiments.

Supplementary Material Available: Tables of temperature factors, atomic parameters, bond lengths, and bond angles for $[Fe_2(CO)_{6-n}\{P(OMe)_3\}_n\{\mu\text{-}(CF_3)C_2(CF_3)S\}]$, $n = 1$–3 (14 pages). Ordering information is given on any current masthead page.

OM920285R